Zonal expression of StARD1 and oxidative stress in alcoholic-related liver disease

Raquel Fucho[1,2,3,4,‡], Estel Solsona-Vilarrasa[1,2,3,4,‡], Sandra Torres[1,2,3,4], Susana Nuñez[1,2,3,4], Naroa Insausti-Urkia[1,2,3,4], Albert Edo[1,2,3,4], Maria Calvo[5], Anna Bosch[5,†], Gemma Martin[5], Carlos Enrich[3,6,7], Carmen García-Ruiz[1,2,3,4,*], and Jose C. Fernandez-Checa[1,2,3,4,8,*]

[1]Department of Cell Death and Proliferation, Institute of Biomedical Research of Barcelona (IIBB), CSIC, Barcelona, Spain; [2]Liver Unit, Hospital Clinic I Provincial de Barcelona, Barcelona, Spain; [3]Instituto de Investigaciones Biomédicas August Pi i Sunyer (IDIBAPS), Barcelona, Spain; [4]CIBEREHD, Madrid, Spain; [5]Advanced Optical Microscopy-Clinic Campus, Scientific and Technological Center, and [6]Unit of Cell Biology, Departament of Biomedicine, Faculty of Medicine and Health Sciences, University of Barcelona, Barcelona, Spain; [7]Center of Biomedical Research CELLEX, Barcelona, Spain; [8]Department of Medicine, Keck School of Division of Gastrointestinal and Liver Disease, University of Southern California, Los Angeles, CA, USA

Abstract Alcoholic-related liver disease (ALD) is one of the leading causes of chronic liver disease and morbidity. Unfortunately, the pathogenesis of ALD is still incompletely understood. StARD1 has emerged as a key player in other etiologies of chronic liver disease, and alcohol-induced liver injury exhibits zonal distribution. Here, we report that StARD1 is predominantly expressed in perivenous (PV) zone of liver sections from mice-fed chronic and acute-on-chronic ALD models compared to periportal (PP) area and is observed as early as 10 days of alcohol feeding. Ethanol and chemical hypoxia induced the expression of StARD1 in isolated primary mouse hepatocytes. The zonal-dependent expression of StARD1 resulted in the accumulation of cholesterol in mitochondria and increased lipid peroxidation in PV hepatocytes compared to PP hepatocytes, effects that were abrogated in PV hepatocytes upon hepatocyte-specific *Stard1* KO mice. Transmission electron microscopy indicated differential glycogen and lipid droplets content between PP and PV areas, and alcohol feeding decreased glycogen content in both areas while increased lipid droplets content preferentially in PV zone. Moreover, transmission electron microscopy revealed that mitochondria from PV zone exhibited reduced length with respect to PP area, and alcohol feeding increased mitochondrial number, particularly, in PV zone. Extracellular flux analysis indicated lower maximal respiration and spared respiratory capacity in control PV hepatocytes that were reversed upon alcohol feeding. These findings reveal a differential morphology and functional activity of mitochondria between PP and PV hepatocytes following alcohol feeding and that StARD1 may play a key role in the zonal-dependent liver injury characteristic of ALD.

Supplementary key words mitochondria • cholesterol • oxidative stress • alcoholic-related liver disease

Alcoholic-related liver disease (ALD) is a leading cause of chronic liver disease and related mortality in Western countries caused by excessive consumption of alcohol. ALD encompasses a spectrum of liver alterations, ranging from steatosis to alcoholic steatohepatitis, which can further progress to advanced stages such as cirrhosis and hepatocellular carcinoma (1–3). Alcohol is metabolized in the liver by alcohol dehydrogenase resulting in the generation of acetaldehyde, which in turn can be oxidized to acetate by acetaldehyde dehydrogenase (ALDH) (4, 5). Alternatively, alcohol can be also metabolized via the microsomal cytochrome P450 system, with CYP2E1 playing a crucial role due to its upregulation by chronic alcohol intake. The oxidative metabolism of alcohol through either alcohol dehydrogenase or CYP2E1 generates superoxide anion and other reactive oxygen species (ROS), which can inflict harmful effects in hepatocytes, and nonparenchymal cells (e.g., Kupffer cells, endothelial cells, and hepatic stellate cells) (5, 6). The onset of oxidative stress along with other players, such as endoplasmic reticulum (ER) stress, disruption of methionine metabolism, genetic and environmental

‡These authors contributed equally to this work.
†Deceased during the performance of this study.
*For correspondence: Jose C. Fernandez-Checa, checa229@yahoo.com; Carmen García-Ruiz, cgrbam@iibb.csic.es.

© 2023 THE AUTHORS. Published by Elsevier Inc on behalf of American Society for Biochemistry and Molecular Biology. https://doi.org/10.1016/j.jlr.2023.100413
This is an open access article under the CC BY-NC-ND license (http://creativecommons.org/licenses/by-nc-nd/4.0/).

factors, and mitochondrial dysfunction can elicit adverse responses, such as hepatocellular death, inflammation, and fibrosis, which contribute to the progression of ALD to advanced stages (4–8).

Alcohol metabolism regulates hepatic lipid metabolism leading to an imbalance between the biogenesis and catabolism of lipids that translates in the initial stage of hepatic steatosis (9). In addition, alcohol increases hepatic cholesterol levels, which can aggravate ALD progression (10). Recent findings indicated that the inactivation of ALDH2, the enzyme responsible for alcohol flux in nearly 8% of the world population and about 40% of Asians, increases the expression of 3-hydroxy-3-methylglutaryl-CoA reductase, the rate-limiting step in the de novo synthesis of cholesterol (11). The ALDH2-mediated regulation of cholesterol synthesis is linked to the mitochondria-associated ER membranes, a specific domain of membranes in which ER and mitochondria contact, which plays a critical role in the transfer of calcium and lipids, including cholesterol between ER and mitochondria (12, 13). In line with these findings, previous studies indicated that alcohol intake triggered the enrichment of cholesterol in mitochondria, which negatively regulates the homeostasis of mitochondrial antioxidant strategies in ALD, such as mitochondrial GSH redox cycle (6, 14–18). Alcohol-induced mitochondrial GSH depletion contributes to liver injury by sensitizing hepatocytes to secondary insults and inflammatory cytokines-mediated cell death (19, 20).

Moreover, mitochondrial dysfunction plays a role in ALD pathogenesis and cholesterol accumulation in mitochondria impairs mitochondrial function (21–23). Thus, uncovering the mechanism for the trafficking of cholesterol to mitochondria may represent a significant advance in understanding ALD pathogenesis. Besides vesicle-mediated interorganellar transport, intracellular cholesterol trafficking can occur through a non-vesicular protein-mediated transfer mechanism in membrane contact sites, in which specific proteins work as cholesterol transporters due to the presence of lipid-binding pocket domains (24, 25). In this regard, steroidogenic acute regulatory protein 1 (StARD1), plays a crucial role in the delivery of cholesterol to mitochondrial inner membrane for metabolism and has emerged as a key player in liver diseases, including drug-induced liver injury and nonalcoholic steatohepatitis-driven hepatocellular carcinoma (26–28).

The liver exhibits metabolic zonation, with the segregation of hepatocyte populations involved in specialized functions that are largely determined by anatomical features (29–31). In this regard, expression of CYP2E1 is enriched in the perivenous (PV) zone of the liver, coinciding with the area being most sensitive to the damaging effects of chronic alcohol intake (32–34). In addition, mitochondrial GSH depletion has been reported preferentially in PV compared to periportal (PP) hepatocytes from rats fed alcohol (35, 36). However, whether StARD1 is expressed in a zonal-dependent pattern has not been previously reported, and thus, we examined the expression of StARD1 and mitochondrial function in PP and PV hepatocytes in ALD.

MATERIALS AND METHODS

Animals and ALD models

Wild type C57BL/6J male mice (8–10 week old) were obtained from Charles River Laboratories (Wilmington, MA). Mice with hepatocyte-specific StARD1 (*Stard1*$^{\Delta hep}$) deletion have been generated and characterized as described recently (27). To model chronic ALD, mice were randomly separated in two groups that were fed with a Lieber-DeCarli liquid diet (Research Diets, cat no: L10016A) with maltodextrin (CTRL) or 5% ethanol for 10 or 30 days. In addition, we used the acute-on-chronic NIAAA model (37) and pair-fed control or ethanol-containing Lieber-DeCarli liquid diets (Research Diets, cat no: L10016A), providing 36% of calories from ethanol (or maltose), as previously described (37, 38). After 10 days of chronic alcohol feeding, mice were gavaged with alcohol (5 g/kg) and euthanized 8 h later. Animals were housed in temperature-and humidity-controlled rooms and kept on a 12 h light/dark cycle. All the experimental protocols used were approved and performed in accordance with the Animal Care Committee of the Hospital Clinic-Universidad de Barcelona and conformed to the highest international standards of humane care of animals in biomedical research.

Isolation of PP and PV hepatocytes

Livers were extracted from mice for whole liver analysis. PP and PV mouse hepatocytes were prepared through perfusion of portal and superior cava veins followed by a dual digitonin-collagenase digestion, as previously described (35, 36). Briefly, for zone-specific cell destruction, digitonin was infused for 10 s in the prograde or retrograde direction to prepare PP and PV hepatocytes, respectively. Immediately after the infusion of digitonin, Hanks's buffer was infused through the opposite cannula for 2–3 min, followed by collagenase (100 units/ml) perfusion with Hank's buffer supplemented with 2.5 mM $CaCl_2$. Hepatocytes were then cultured at a density of 1×10^6–70×10^3 cells per 60 mm dish or a 12-well plate coated with rat-tail collagen. Hepatocytes were cultured in DMEM/F12 culture media (Gibco, 21331-020) supplemented with 10% FBS, 100 U/ml Penicillin-Streptomycin (Gibco, 15140-122), 2 mM L-Glutamine (Gibco, 25030-024), and 150 mM Hepes pH 7.4 (Sigma-Aldrich) for the first 3 h post isolation. Medium without FBS was used for subsequent treatments. The quality of the PP and PV populations of hepatocytes was verified by the determination of the expression of specific markers for either zone, including E-cadherin and CYP2F2 for PP area, and CYP2E1 and glutamine synthase (GLUL) for the PV zone (29–31). In some cases, PV hepatocytes were isolated from *Stard1*$^{\Delta hep}$ mice fed liquid diet containing 5% ethanol to determine the impact of alcohol feeding on mitochondrial cholesterol, GSH homeostasis, oxidative stress, and mitochondrial ultrastructure.

In vitro treatment of primary mouse hepatocytes

To assess the effects of hypoxia and ethanol in primary mouse hepatocytes (PMH), cultured PMH were treated with

ASBMB

100 μM $CoCl_2$ and/or 100 mM ethanol for 24 h. Hypoxia-inducible factor (HIF) and StARD1 expression were determined by Western blot analyses. For ROS generation determination, cultured PMH were incubated in dichloro fluorescein diacetate (10 μM) solution for 30 min at 37°C in dark. Cells were then washed with PBS and evaluated by fluorescence spectroscopy using the Synergy HT multi-mode microplate reading (485 nm for excitation and 528 nm for emission). The fluorescence was normalized by protein content, determined by BCA protein assay. The induction of reactive species was calculated with respect to control samples.

Mitochondrial isolation

Mitochondria were isolated by differential centrifugation, as previously described (19, 20). Briefly, livers were minced in 10 volume of cold buffer A (225 mM mannitol, 75 mM sucrose, 0.1 mM EGTA, 10 mM Hepes, and 1 mg/ml fatty acid-free BSA, pH 7.4) supplemented with protease and phosphatase inhibitors (Roche). After tissue disruption, mitochondria fraction was isolated by differential centrifugation, 15 min at 700 g followed by 15 min at 10,000 *g* at 4°C. Pellets containing mitochondria were resuspended in Buffer B (395 mM sucrose, 0.1 mM EGTA, and 10 mM Hepes, pH 7.4). Alternatively, mitochondrial fractions for GSH determination from PMH were prepared by digitonin fractionation to selectively disrupt plasma membrane, as described previously (35, 36). Briefly, PMH (1×10^6 cells) in 0.1 ml Hepes buffer (19.8 mM EDTA, 250 mM mannitol in 17.0 mM Hepes, pH 7.4) containing 0.24 mg/ml digitonin were added to a 0.5 ml silicone-mineral oil mixture layer and centrifuged at 13,000 *g* in microfuge at room temperature for 3 min.

Extracellular flux analysis

Mitochondrial suspensions in 70 mM sucrose, 220 mM mannitol, 10 mM KH_2PO_4, 5 mM $MgCl_2$, 2 mM Hepes, 1.0 mM EGTA, and 0.2% (w/v) fatty acid-free BSA, pH 7.2 were incubated with either pyruvate and malate (10 mM) or succinate (10 mM) and rotenone (2 μM) as substrates for respiration and delivered to XFe24 Seahorse plates and loaded into the XFe24 Analyzer for mitochondrial respiration analysis, as described previously (21). Real-time determination of oxygen consumption rates (OCR) from PP and PV hepatocytes was determined by a sequential injection of 2 μM oligomycin, 0.2 μM carbonyl cyanide 4-(trifluoromethoxy) phenylhydrazone, and 2 μM antimycin A plus rotenone, as previously described (39).

Transmission electron microscopy

Mice were perfused through the portal vein to wash the liver with cold saline and then fixed by perfusion with 2.5% glutaraldehyde in phosphate buffer. Liver tissue fragments were extracted and fixed with 2.5% glutaraldehyde and 2% paraformaldehyde in phosphate buffer (0.1 M; pH 7.4), post fixed in 1% osmium tetroxide and 0.8% potassium ferrocyanide, dehydrated with acetone, and embedded in epoxy resin. Semithin sections were cut and stained with methylene blue for light microscopy to select PP and PV areas. Ultrathin sections (70 nm) for transmission electron microscope (TEM) were cut, collected in 100-mesh cooper grids and stained with 2% uranyl acetate for 10 min and with a lead-staining solution for 2 min. Images from stained ultrathin sections were acquired using a transmission electron microscope JEOL JEM-1010 fitted with a Gatan Orius SC1000 (model 832) digital camera. ImageJ software (https://imagej.nih.gov/ij/) was used to quantify glycogen and lipid droplets (LDs) content, as well as mitochondrial length and number.

Biochemical determinations

Alanine aminotransferase and aspartate aminotransferase as well as total bile acids (BAs) were analyzed by the Clinical Core Laboratories at the Hospital Clinic i Provincial de Barcelona on an ADVIA 2400 Chemistry System (Siemens Medical Solutions, Erlangen, Germany) using commercially available kits, ADVIA Chemistry System 1650 (Bayer-Siemens) and CHOD-PAP (Roche Diagnostics).

Western blotting

Total liver homogenates and cultured mouse hepatocytes were diluted with RIPA lysis buffer (Sigma-Aldrich) with antiproteases and antiphosphatases. Samples were incubated 15 min at 4°C, vortexed, and spanned down for 10 min at 10,000 rpm. All supernatants were collected and quantified for protein concentration using Pierce BCA Protein Assay Kit (Thermo Fisher Scientific). Between 20 and 50 μg of protein were subjected to 4%–12% SDS–polyacrylamide gel electrophoresis (SDS-PAGE) (Bio-Rad, XT-Criterion) and then electrotransferred onto nitrocellulose membranes (Bio-Rad). One percent–five percent BSA solution in TBS-Tween was used to block the membranes for 1 h at room temperature. Membranes were incubated overnight with the following primary antibodies: CYP2E1 (Abcam, ab28146), CYP2F2 (Santa Cruz, sc374540), E-Cadherin (Santa Cruz, sc59778), FIS1 (Abcam, ab71498), GLUL (Abcam, ab73593), HIF2α (Abcam, ab109616), 4HNE (Abcam, ab46545), StARD3 (Santa Cruz, sc292868), OPA1 (Abcam, ab42364), Porin (Merck Millipore, MABN504), StARD1 (Cell Signaling, #8449), β-Actin (Sigma-Aldrich, A3854). Membranes were thoroughly washed with TBS-Tween and incubated for 45 min with their respective HRP-conjugated secondary antibodies. Pierce ECL Western Blotting Substrate (Thermo Fisher Scientific) was used to develop the membranes. LAS4000 (GE HealthCare) was used to digitally capture images and absorbance was analyzed with ImageJ software.

Staining of liver sections

For immunohistochemistry analysis paraffin molds containing liver samples were cut into 5-μm sections and mounted on HistoGrip-coated slides. The sections were deparaffinized in xylene and dehydrated in a graded alcohol series. Endogenous peroxidase (3% H_2O_2) and endogenous avidin and biotin were used to block. Slides were incubated with primary antibody (StARD1, Santa Cruz, sc23524) overnight in a wet chamber at 4°C. After washing with PBS, slides were incubated with a biotinylated antibody for 45 min in a wet chamber and developed with an ABC Kit with peroxidase substrate (diaminobenzidine) and peroxidase buffer. After the slides were rinsed with tap water, they were counterstained with hematoxylin and mounted with Aquatex. Olympus BX41 microscope was used to take images.

For immunohistofluorescence analyses, 12-μm liver frozen sections were fixed in 10% formalin for 1 h at room temperature, washed with PBS and blocked with antibody diluent (Abcam ab64211) and 10% Normal Goat Serum ready-to-use (Life technologies #5000627) at room temperature for 20 and 10 min, respectively. Sections were then washed with PBS

and incubated overnight at 4°C with the following primary antibodies: CYP2F2 (Santa Cruz, sc374540), GLUL (Abcam, ab73593), StARD1 (Cell Signaling, #8449), and hydroxyprobe pimonidazole (Hydroxyprobe, Inc, HPI, MAb1). Sections were subsequently washed with PBS, incubated with their respective fluorochrome-conjugated secondary antibodies for 45 min at room temperature and stained with 0.2 mg/ml Filipin in PBS for 3 h at room temperature. Additionally, samples were stained with glutathione-S-transferase tag fused with the perfringolysin O (GST-PFO) to localize cholesterol, as described previously (40). Samples were finally washed with PBS and embedded in fluorescent mounting medium (Dako #S3023) or ProLong™ Diamond Antifade Mountant with DAPI (Invitrogen, P36962) to mount the coverslips. Digital images were taken in a Leica DM2500 confocal microscope. Low magnification (10×) confocal images were obtained in Dragonfly microscope, Andor.

Laser confocal imaging

Cultured PMH were fixed for 15 min with 4% paraformaldehyde and permeabilized and blocked for 15 min with 0.2% saponin dissolved in 1% BSA-fatty acid free in PBS commercial buffer. Cytochrome C (BD Pharmingen, 556432) primary antibody was incubated overnight in BSA 1% followed by a secondary antibody for 1 h at room temperature in BSA 0.1%. Filipin (Sigma-Aldrich) was added at 0.33 mg/ml during the secondary antibody incubation and the following steps were performed in the dark. Stained samples were mounted in Fluoromont (Sigma-Aldrich), and digital images were taken in a Leica DM2500 confocal microscope.

GSH levels determination

Aliquots of one million hepatocytes were taken right after hepatocyte isolation from mice. Cells were then fractionated into cytosol and mitochondria by selectively permeabilizing the plasma membrane with digitonin and subsequent centrifugation through an oil layer with 10% trichloroacetic acid as described (34, 35). Aliquots of the cytosolic and mitochondrial fractions were kept on ice for determination of GSH levels by the recycling method as previously described (41).

Statistical analysis

Statistical analyses were performed using GraphPad Prism 9 (Graphpad Software Inc; https://www.graphpad.com). Unpaired Student's *t* test (two tailed) was performed between two groups and one or two-way ANOVA followed by Tukey's multiple comparison tests were used for statistical comparisons between three or more groups. The corresponding number of experiments is indicated in the figure legends. Data in graphs are shown as mean ± SEM.

RESULTS

Chronic and acute-on-chronic alcohol intake increases StARD1 expression in a zonal-dependent manner

Previous studies indicated that alcohol feeding to mice increases the expression of StARD1 (18). However, whether this event occurs in a zonal-dependent manner was not investigated. Thus, we fed mice a liquid diet containing ethanol (5%) for 10 and 30 days to examine the zonal distribution of StARD1. Although feeding mice alcohol for 30 days markedly altered the liver architecture, with centrilobular hepatocyte hypertrophy and hepatic macrovesicular steatosis, 10 days of feeding already caused liver injury and microvesicular steatosis (supplemental Fig. S1). Chronic alcohol feeding for 30 days increased the expression of StARD1 in parallel with the increase of CYP2E1, and this effect was observed as early as 10 days of alcohol feeding (**Fig. 1**A–D), suggesting that the expression of StARD1 is an early event in ALD. In contrast, hepatic expression of StARD3, also known as MLN64, did not change in extracts from alcohol-fed mice (supplemental Fig. S2). Immunohistochemical staining of liver sections from mice fed with alcohol revealed a zonal-dependent pattern of StARD1 distribution, exhibiting higher expression around the central vein, suggesting preferential expression in the PV zone (Fig. 1E). To further confirm the zonal-dependent expression of StARD1, we performed immunofluorescence analyses of liver sections stained with GLUL antibody to identify areas enriched in glutamine synthase, a PV marker and StARD1 antibody (30, 31). As seen, while the expression of StARD1 in liver sections from control mice was barely detectable consistent with the low basal expression of StARD1 in the liver, alcohol feeding for 10 or 30 days increased StARD1 expression that colocalized with GLUL stained areas (Fig. 1F, G; see also supplemental Fig. S3), indicating that alcohol induced the expression of StARD1 preferentially in PV areas. Furthermore, we next examined whether this pattern of expression was also observed in a more severe model of ALD. Mice fed acute-on-chronic NIAAA alcohol model exhibited increased expression of StARD1 that colocalized with GLUL-stained area (Fig. 1H and supplemental Fig. S3). Taken together these findings indicate that chronic alcohol intake leads to a preferential expression of StARD1 in PV zone.

Predominant expression of StARD1 in isolated PV hepatocytes from alcohol-fed mice

To further verify the zonal-dependent pattern of StARD1 expression in ALD, we next isolated PP and PV hepatocyte populations from alcohol-fed mice using a dual digitonin-collagenase perfusion approach and examined expression of zone-specific markers (see Methods for details). As seen, E-cadherin, a PP marker, was enriched in PP hepatocytes with barely expression in PV population, while GLUL expression was higher in PV hepatocytes (**Fig. 2**A–D). The zone-specific enrichment was maintained in PP and PV hepatocytes from alcohol-fed mice, although the levels of both E-cadherin and GLUL were somewhat reduced compared to control PP and PV hepatocytes. As expected, Western blots showed that the expression of CYP2E1 was significantly enhanced following alcohol feeding in both populations, with a higher level of expression in PV hepatocytes compared to PP hepatocytes, further

ASBMB

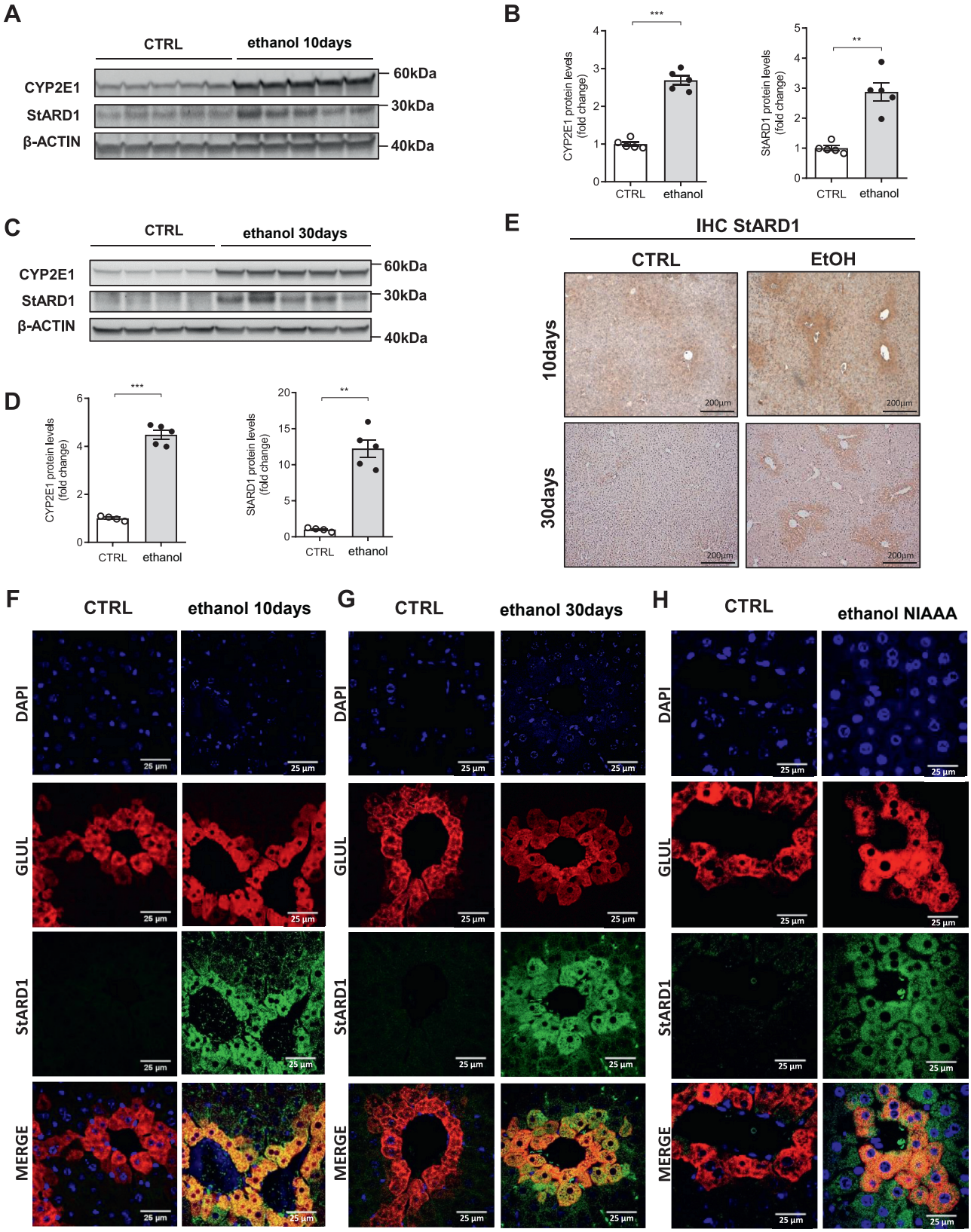

Fig. 1. Effects of alcohol consumption on the expression of StARD1. WT C57BL/6 mice were exposed to Lieber-DeCarli diet with maltodextrin (CTRL) or 5% ethanol for 10 or 30 days. A, C: immunoblotting of liver homogenates showing the protein expression of StARD1 and CYP2E1 at 10 and 30 days. Quantification is shown in (B) and (D) by ImageJ software. β-Actin was used as loading control. Images are representative of at least three independent experiments. Values are the mean ± SEM of >5 animals per group. $P < 0.05$. Unpaired Student's t test (two tailed). E: StARD1 levels and distribution in the liver by immunohistochemistry of StARD1 at 10 or 30 days after ethanol feeding. Bar scale = 200 μm. F: Characterization of subcellular localization of GLUL and StARD1 in mouse liver. Representative immunohistofluorescence images from at least 3 replicates per group at 10 days after ethanol feeding. Bar scale = 25

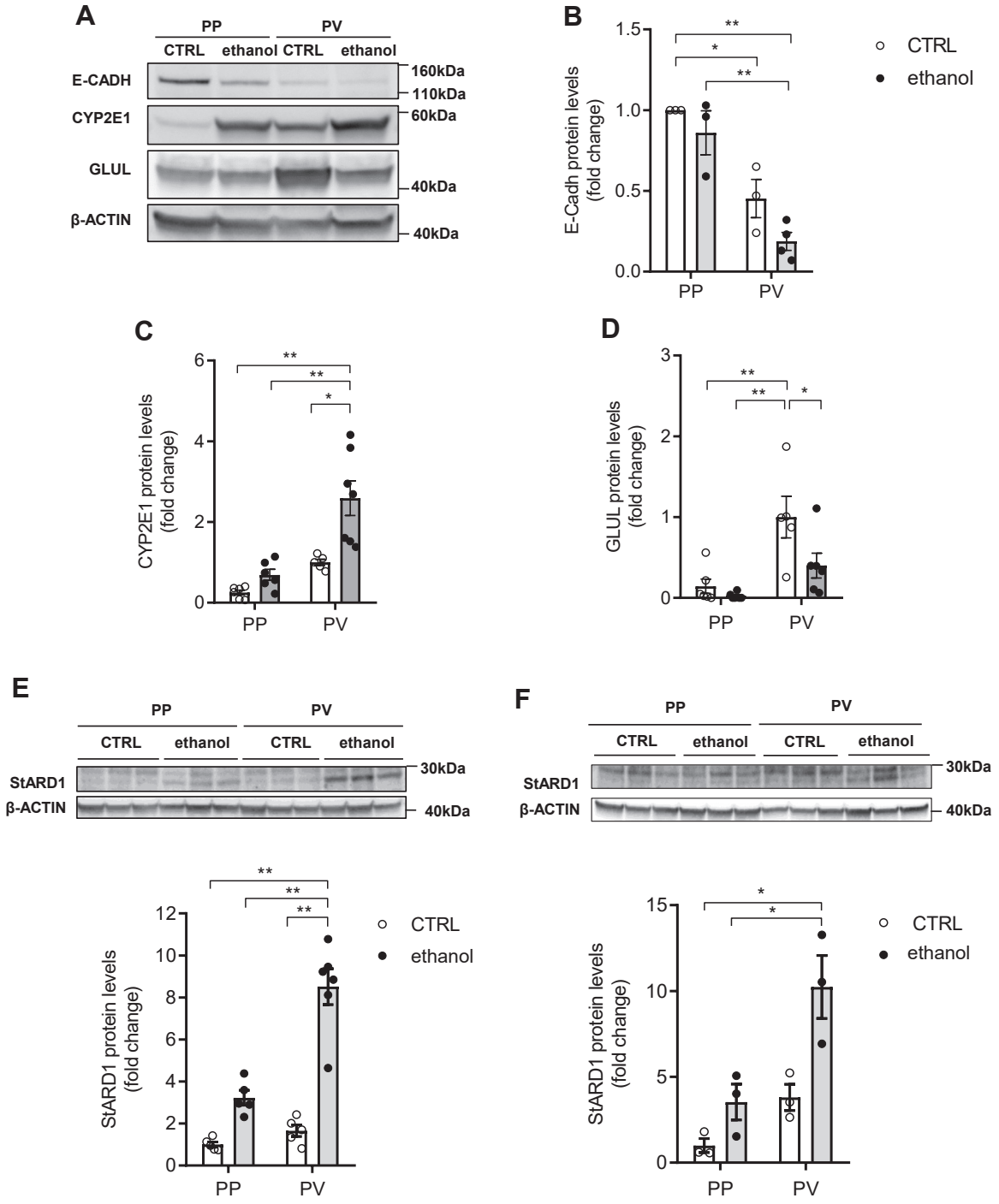

Fig. 2. Differential expression of StARD1 in PP and PV hepatocytes. A: Western blot of homogenates from isolated hepatocytes showing protein levels of population enrichment markers (PP: ECADH; PV: CYP2E1 and GLUL). B–D: Protein expression quantification of (A) by ImageJ software. E, F: StARD1 protein levels in CTRL or ethanol PP and PV hepatocytes and protein expression quantification by ImageJ software at 10 days or 30 days ethanol feeding. Data are presented as means ± SEM (N > 6, $P < 0.05$, Two-way ANOVA, (B (diet: F = 5.095, P = n.s.; zonality: F = 45.98, $P < 0.001$; interaction F = 0.48, P = n.s.), C (diet: F = 14.25, $P = 0.001$; zonality: F = 24.33, $P < 0.001$; interaction F = 4.609, $P < 0.05$), D (diet: F = 6.182, $P < 0.05$; zonality: F = 18.07, $P < 0.001$; interaction F = 2.72, P = n.s.), E (diet: F = 69.94, $P < 0.001$; zonality: F = 29.94, $P < 0.001$; interaction F = 18.21, $P < 0.001$) and F (diet: F = 15.47, $P < 0.01$; zonality: F = 17.37, $P < 0.01$; interaction F = 2.926, P = n.s.)) followed by Tukey's multiple comparison test). GLUL, glutamine synthase; PP, periportal; PV, perivenous; StARD1, steroidogenic acute regulatory protein.

μm. G: The same at 30 days after ethanol feeding. Bar scale = 25 μm. H: Representative immunohistofluorescence images from at least 3 replicates per group after NIAAA ethanol feeding model. Bar scale = 25 μm. Values are the mean ± SEM (N > 3, $P < 0.05$, Two-way ANOVA followed by Tukey's multiple comparison test). GLUL, glutamine synthase; StARD1, steroidogenic acute regulatory protein.

indicating segregation of PP and PV-enriched hepatocyte populations (Fig. 2A, C). Consistent with the immunohistochemical and immunofluorescence analyses of liver sections, StARD1 expression by alcohol feeding was higher in isolated PV hepatocytes compared to PP population, and this outcome was observed as early as 10 days of alcohol intake (Fig. 2E, F). Like in cell extracts, expression of StARD3 in PP and PV hepatocytes was unchanged in alcohol-fed mice (supplemental Fig. S2). Thus, taken together StARD1 exhibits a zonal-dependent pattern of expression following chronic alcohol feeding with a predominant induction in PV zone.

Hypoxia synergizes with alcohol to induce StARD1 expression in PMH

We next explored the mechanism whereby alcohol feeding increases StARD1 in PV hepatocytes. PV zone is not only enriched in CYP2E1 expression but exhibits a lower oxygen tension compared with PP area and it is the area where HIFs are mainly activated (28–31). Hence, we examined the impact of hypoxia and alcohol in the expression of StARD1 in PMH. Exposure of PMH to chemical hypoxia with $CoCl_2$ induced HIF2α, as expected, that was further potentiated by simultaneous incubation with ethanol (**Fig. 3**A, B). While this synergism did not affect the expression of CYP2E1 (Fig. 3A, C), it did increase that of StARD1 (Fig. 3A, D). In line with the findings in PMH, staining of liver sections with the hydroxyprobe pimonidazole to detect hypoxic areas and anti-GLUL antibody indicated that alcohol feeding exacerbated the onset of hypoxia in areas that colocalized with GLUL (Fig. 3E). As ER stress is a major player in ALD and HIF is known to increase the expression of *Stard1* at the transcriptional level (18, 27, 42), our findings indicate that alcohol and HIF stabilization synergize to induce the expression of StARD1.

Alcohol feeding increases hepatic and mitochondrial cholesterol in PV zone

Alcohol metabolism alters the imbalance between the biosynthesis and catabolism of lipids leading to hepatic steatosis (9). In addition to the increase in triglycerides, a major component of the LDs characteristic of macrovesicular hepatic steatosis, alcohol intake also has been shown to increase the cholesterol content (10, 14). To examine whether alcohol feeding increases cholesterol levels even after a 10-day period, we stained liver sections with GST-PFO, a stable and specific probe that labels membrane cholesterol (40). Consistent with previous observations (10, 14), liver sections stained with GST-PFO indicated a higher cholesterol level in mice fed alcohol compared to sections from control mice (**Fig. 4**A). Moreover, GST-PFO staining colocalized with sections labeled with GLUL to detect PV areas, indicating a predominant increase of cholesterol in PV zone after alcohol feeding (Fig. 4A). Similar findings showing predominant increase of cholesterol in PV were observed when liver sections were stained with filipin, an antibiotic that detects free cholesterol, and GLUL or CYP2F2 antibodies to delineate PV and PP zones, respectively (supplemental Fig. S4). Besides increasing cholesterol levels in liver sections of mice fed alcohol, we next examined the content of cholesterol in mitochondria. Thus, isolated PP and PV hepatocytes from control and alcohol-fed mice were stained with filipin to detect cholesterol and cytochrome c to label mitochondria. Laser confocal analyses revealed a higher degree of colocalization of filipin with cytochrome c in PV hepatocytes than PP hepatocytes from alcohol-fed mice (Fig. 4B). Thus, these findings indicate that in line with the increase of cholesterol following alcohol intake mitochondrial cholesterol preferentially accumulates in PV hepatocytes.

Alcohol feeding induces mitochondrial GSH depletion and oxidative stress in a zonal-dependent manner

As StARD1 mediates mitochondrial cholesterol loading, which in turn, has been described to regulate the transport of GSH into mitochondria (14, 21, 25), we next determined the zonal distribution of mitochondrial GSH levels following alcohol intake. Mitochondrial GSH levels were determined in isolated PP and PV hepatocytes after permeabilization with digitonin and subsequent centrifugation through oil layer as described previously (35, 36). Determination of GSH in the mitochondrial fractions revealed a preferential depletion in PV hepatocytes from alcohol-fed mice with respect to PP population (**Fig. 5**A), in line with previous reports in alcohol-fed rats (35, 36). These findings suggest that the preferential depletion of mitochondrial GSH in PV zone by alcohol intake in mice is species independent. As GSH is a crucial mitochondrial antioxidant defense, we next examined the zonal distribution of lipid peroxidation. As seen, 4-hydroxynonenal (4-HNE) levels were higher in PV hepatocytes from alcohol-fed mice compared to PP population (Fig. 5B), correlating with the predominant depletion of mitochondrial GSH content. Moreover, ROS determined by dichlorofluorescein diacetate fluorescence indicated higher oxidative stress in PV hepatocytes from alcohol-fed mice (Fig. 5C). Thus, these findings revealed that alcohol intake caused a selective depletion of mitochondrial GSH and increased oxidative stress in the PV zone of the liver, coinciding with the area exhibiting more alcohol-related liver injury.

Unchanged zonal distribution of BAs in alcohol-fed mice

Cholesterol is a precursor for BAs, which can be synthesized via the classic and alternative mitochondrial pathways, the latter being regulated by StARD1-mediated cholesterol trafficking to mitochondria (43–46). BAs can be potentially toxic and alcohol

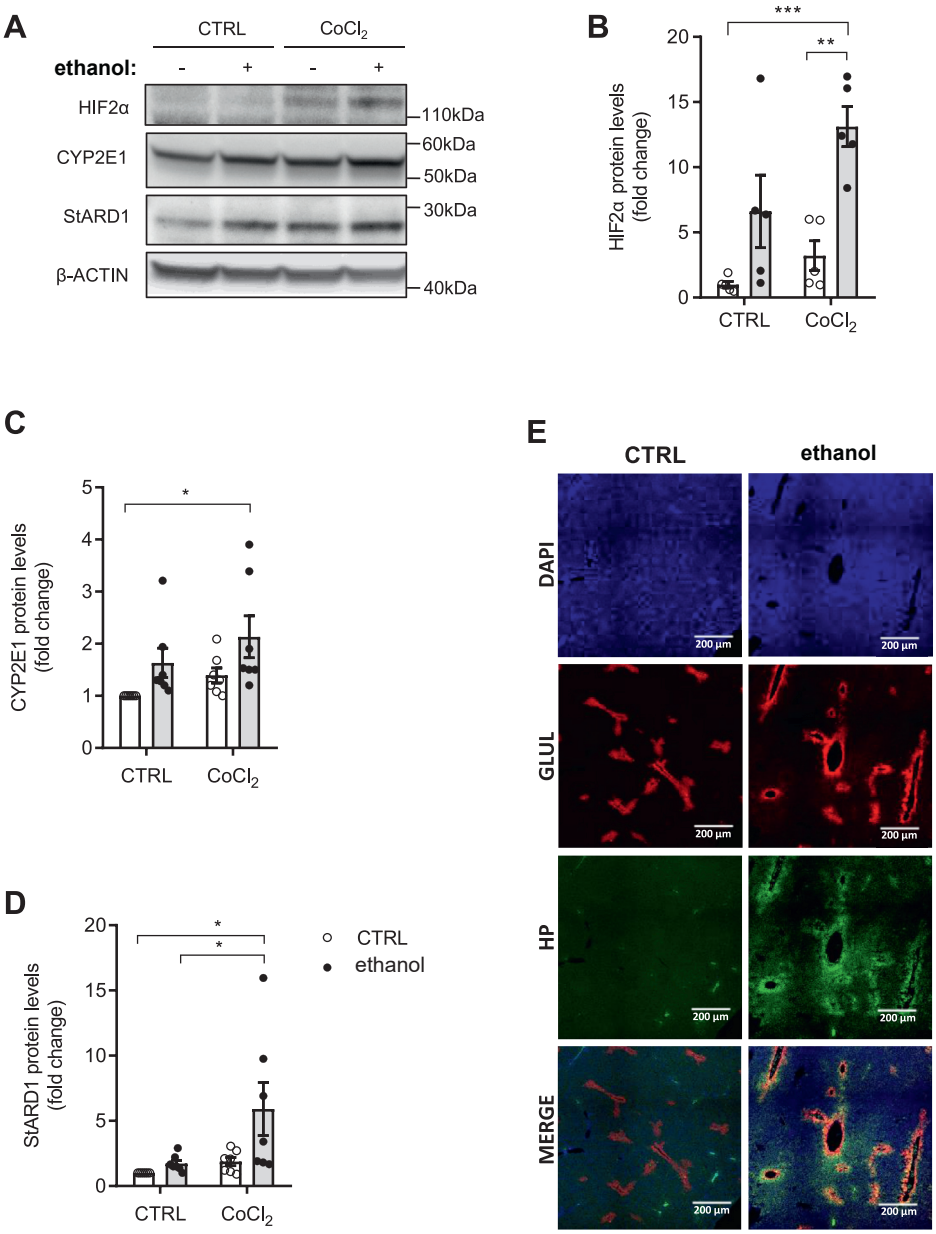

Fig. 3. Chemical hypoxia and alcohol synergize to induce the expression of StARD1. A: Western blot of homogenates from mouse primary hepatocytes, treated for 24 h with 100 µM $CoCl_2$ and/or 100 mM ethanol, showing protein expression levels of HIF2α, CYP2E1, and StARD1. B–D: Protein expression quantification by ImageJ software. E: Liver sections stained with GLUL, DAPI, and hydroxyprobe pimonidazole to identify hypoxic areas. Scale bar, 200 µm. Values are the mean ± SEM of >10 animals per group. $P < 0.05$. Two-way ANOVA (B (ethanol: F = 20.95, $P < 0.001$; hypoxia: F = 6.622, $P < 0.05$; interaction F = 1.608, P = n.s.), C (ethanol: F = 7.181, $P < 0.05$; hypoxia: F = 3.034, P = n.s.; interaction F = 0.042, P = n.s.), and D (ethanol: F = 5.3, $P < 0.05$; hypoxia: F = 5.954, $P < 0.05$; interaction F = 2.543, P = n.s.)) followed by Tukey's multiple comparison test. DAPI, 4',6-diamidino-2-phenylindole; GLUL, glutamine synthase; HIF, hypoxia-inducible factor; StARD1, steroidogenic acute regulatory protein.

consumption causes cholestasis whose contribution to ALD progression is unclear (47). Moreover, the effect of alcohol intake in the expression of enzymes involved in BAs biosynthesis is controversial (48–51). Thus, we next examined whether the alcohol-induced stimulation of StARD1-mediated cholesterol trafficking to mitochondria translated in higher BAs content in a zonal-dependent manner. Total pool of BAs was unchanged by alcohol feeding in PP and PV hepatocytes from alcohol-fed mice (supplemental Fig. S5A). Moreover, except for the expression of CYP7B1, which was markedly reduced in PP and PV hepatocytes from alcohol-fed mice, and CYP7A1 that was stimulated in PV hepatocytes from control mice, alcohol feeding did not change the expression of CYP27A1 and CYP8B1, involved in the alternative and classic pathways of BAs synthesis, respectively (supplemental Fig. S5B–E). Thus, despite alcohol-induced StARD1 expression and

ASBMB

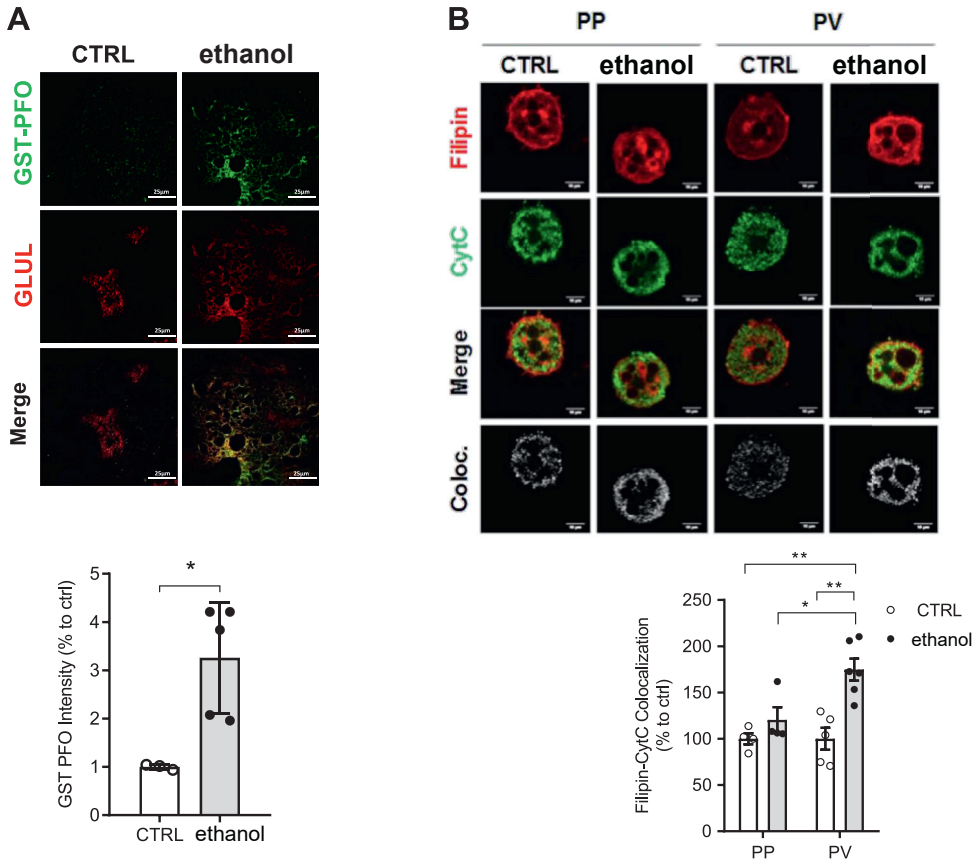

Fig. 4. Alteration of hepatic and mitochondrial cholesterol levels in PP and PV hepatocytes. WT C57BL/6J mice were fed a CTRL or ethanol diet for 10 days. A: Double labeling of control (CTRL) and ethanol (10 days) liver sections for cholesterol levels by GST-PFO staining (green) and anti-GLUL (red). Bar scale = 25 μm. B: Mitochondrial cholesterol levels were analyzed in PP and PV hepatocytes by immunocytochemistry using anti-CytC and Filipin. Bar scale = 10 μm. Staining markers colocalization was analyzed using ImageJ software. Data are presented as means ± SEM (N > 5, $P < 0.05$, Two-way ANOVA (B (diet: F = 16.03, $P < 0.05$; zonality: F = 5.235, $P < 0.05$; interaction F = 5.235, $P < 0.05$)) followed by Tukey's multiple comparison test). GLUL, glutamine synthase; GST-PFO, glutathione-S-transferase tag fused with the perfringolysin O; PP, periportal; PV, perivenous.

mitochondrial cholesterol accumulation in PV zone, alcohol feeding does not lead to a zonal-dependent change in the total pool of BAs.

TEM reveals zonal-dependent alterations in LD population and mitochondrial morphology in alcohol-fed mice

We next examined the structural morphology of PP and PV zones of liver sections from alcohol-fed mice by TEM. First, to ensure that ultrathin sections contained both PP and PV areas, semithin (1 µm) slices were carefully selected under a light microscope (to determine whether the right area of liver samples were in a position for thin sectioning); then, ultrathin sections (70 nm) were cut and placed onto grids (supplemental Fig. S6). Chronic alcohol drinking is known to alter the ultrastructure of hepatocytes affecting the content of glycogen and the presence of LD, characteristic of hepatic steatosis, the initial stage of ALD. While liver sections from control mice presented high glycogen content and few small LD in both areas, samples from alcohol-fed mice revealed a remarkable reduction in glycogen in both zones, with the almost disappearance of glycogen in the PV area (**Fig. 6**A, B), consistent with the reported impact of alcohol abuse in patients with ALD (52). Quantitative analysis of LD showed minor differences between PP and PV zones in samples from control mice, which changed substantially in sections from alcohol-fed mice, reflected in the zonal-dependent alterations in the number and size of LDs. In particular, PP zone from alcohol-fed mice exhibited a number of LDs that ranged from small to large sizes, while PV zone exhibited an increased number of LD of reduced size (Fig. 6C, D), in line with the known expression of enzymes involved in the lipogenesis in the pericentral hepatocytes (30, 31).

Consistent with the effect of alcohol drinking on the ultrastructure of mitochondria (53), we observed striking changes in the appearance of mitochondrial morphology in PP and PV areas. In PV areas from control samples, mitochondrial length was significantly reduced compared to mitochondria from PP zone (Fig. 6D, E). This feature paralleled the observed increased expression of FIS1, a mitochondrial fission

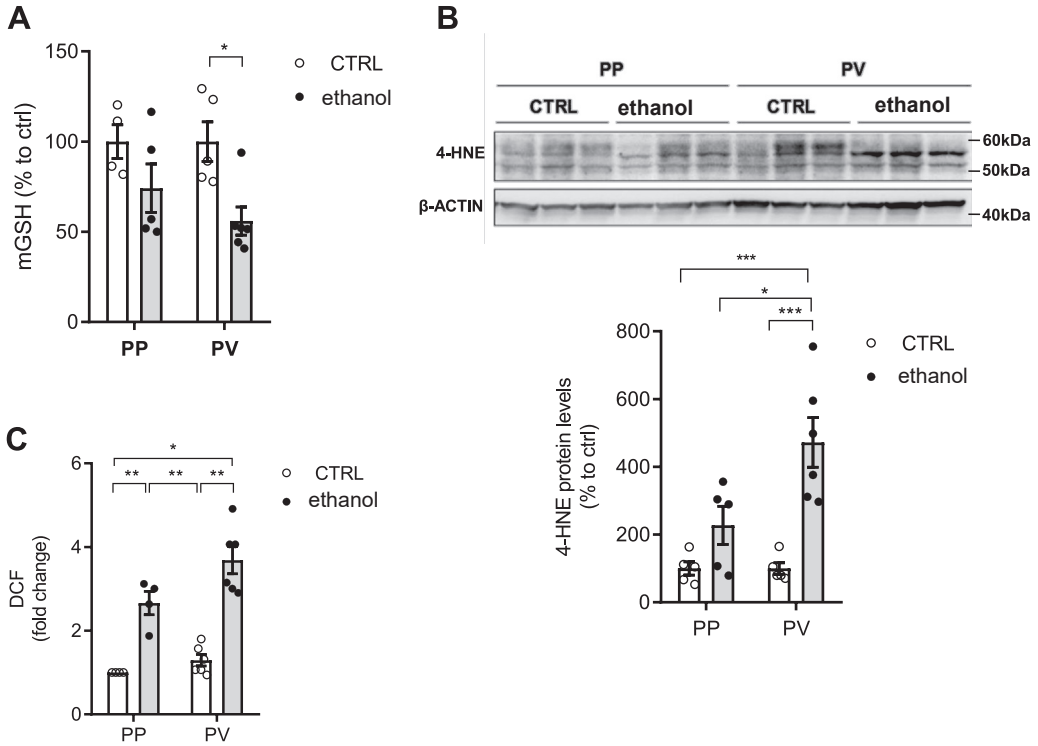

Fig. 5. Mitochondrial GSH status and oxidative stress in PP and PV hepatocytes. WT C57BL/6J mice were fed a CTRL or ethanol diet for 10 days. A: GSH levels in mitochondria. Values are the mean ± SEM of >6 animals per group. $P < 0.05$. Two-way ANOVA followed by Tukey's multiple comparison test. B: Western blot of homogenates from isolated PP and PV hepatocytes with anti-4-HNE protein levels in CTRL or ethanol and protein expression quantification by ImageJ software. C: Reactive oxygen species content in hepatocytes by DCF. Values are the mean ± SEM of >6 animals per group. $P < 0.05$. Two-way ANOVA (A (diet: F = 10.72, $P < 0.01$; zonality: F = 0.791, P = n.s; interaction F = 0.791, P = n.s.), B (diet: F = 23.20, $P < 0.05$; zonality: F = 5.583, $P < 0.05$; interaction F = 5.583, $P < 0.001$) and C (diet: F = 67.61, $P < 0.001$; zonality: F = 7.161, $P < 0.05$; interaction F = 2.199, P = n.s.)) followed by Tukey's multiple comparison test. 4-HNE, 4-hydroxynonenal; DCF, dichlorofluorescein diacetate; PP, periportal; PV, perivenous.

protein without changes in the expression of OPA1 level, in PV with respect to PP zones (supplemental Fig. S7). Ultrastructure analyses in liver sections from alcohol-fed mice revealed an increased mitochondrial number in both zones, particularly in the PV area, with the appearance of larger mitochondria surrounding LD in the PP area (Fig. 6D–F at higher magnification). Moreover, although chronic alcohol feeding did not affect mitochondrial size in PV areas it induced changes in mitochondrial shape with the appearance of concave forms with thick edges and a thin matrix in the center, and donut-like forms with bent shapes shrinking into a ring with a lumen containing cytoplasm (Fig. 6D), consistent with previous findings (54). Furthermore, as shown in other settings such as phenobarbital treatment or drug metabolism/detoxification (55, 56), there were also significant changes in the ER. As seen, the PV zone exhibited more rough endoplasmic reticulum (RER) than PP area in control mice. Interestingly, consistent with the intracellular site where P450 enzymes are expressed (57), chronic alcohol intake caused a shift from RER to a dramatic increase of smooth endoplasmic reticulum (SER) in PV areas, (Fig. 6D, E). These findings underscore zonal-dependent alterations in the ultrastructure of glycogen, LD, and mitochondria after alcohol feeding particularly in the PV zone.

Chronic alcohol feeding induces zonal-dependent alterations in mitochondrial respiration

We next examined the zonal-dependent effects of chronic alcohol feeding on mitochondrial function assessed by extracellular flux analyses. As a first approach, we determined real-time OCR tracings in isolated mitochondria from control and alcohol-fed mice using malate-pyruvate (complex I) or succinate plus rotenone (complex II). While complex I-driven mitochondrial respiration exhibited comparable OCR between control and alcohol-fed mice for 30 days, mitochondria from alcohol-fed mice showed significant increased state 3 respiration with succinate plus rotenone, indicating the stimulation of complex II-driven mitochondrial respiration (**Fig. 7**A, B), in line with recent findings in mitochondria from mice fed alcohol (58–60). To determine the spatial distribution of the effects of alcohol intake on mitochondrial function, we examined OCR in isolated PP and PV hepatocytes from control and alcohol-fed mice. Consistent with the poor oxygen environment of PV zone, PV hepatocytes from control mice displayed significant reduction in functional mitochondrial respiratory parameters, including lower basal respiration, ATP production as well as maximal respiration and spare respiratory capacity compared to PP hepatocytes (Fig. 7C), indicating a spatial

ASBMB

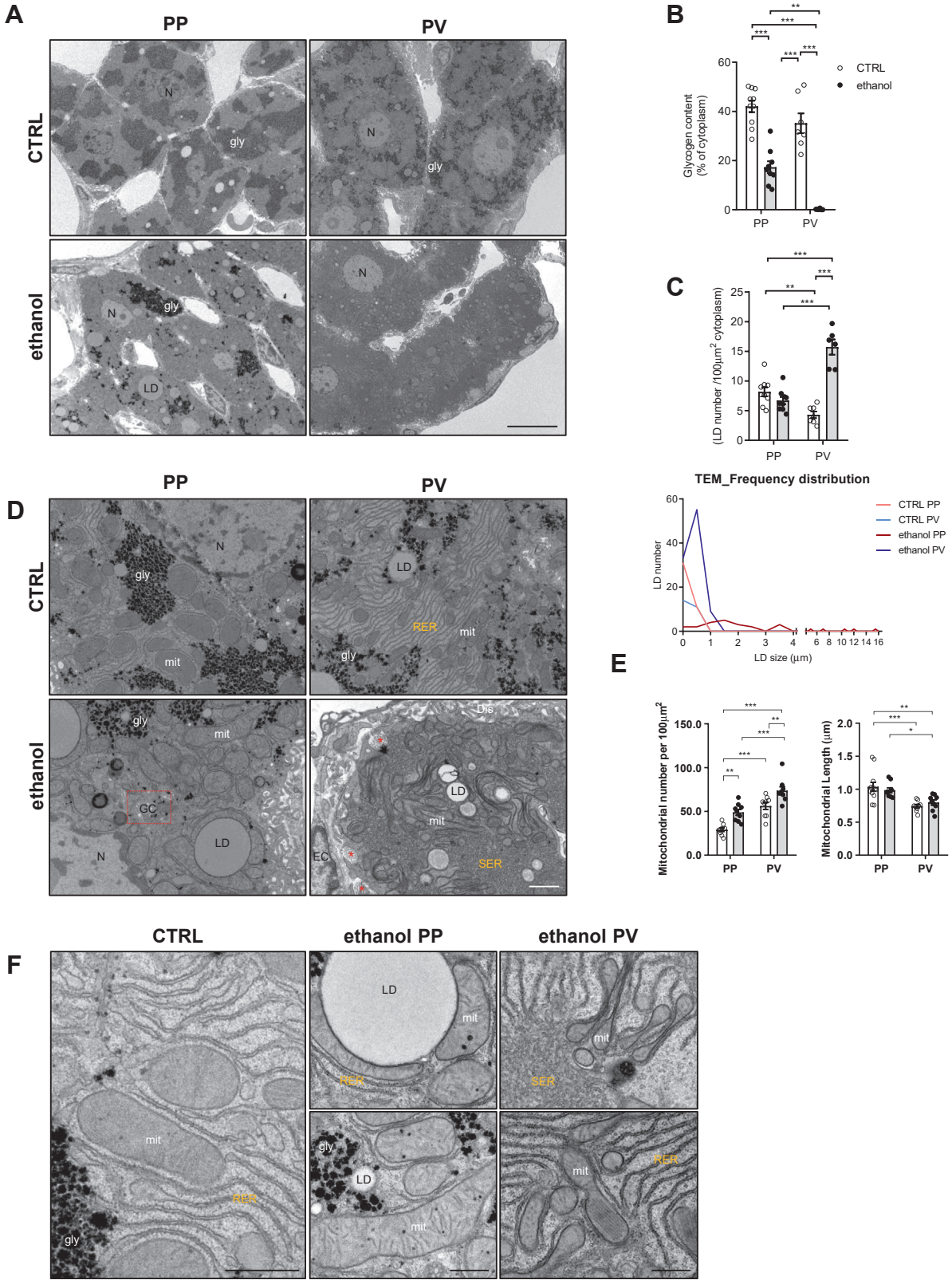

Fig. 6. Ultrastructural alterations in PP and PV areas by chronic alcohol consumption. WT C57BL/6J mice were fed a CTRL or ethanol diet for 30 days. A: Representative images from ultrathin sections, at low magnification, from CTRL or ethanol PP and PV areas taken using a TEM JEOL JEM-1010. gly, glycogen; LD, lipid droplet. Bar scale = 10 μm. B: Quantification of hepatocyte glycogen content. C: Quantification of hepatocyte LD number and LD size distribution among the different populations. N = 3 animals/diet and n ≥ 35 hepatocytes/group. gly, glycogen. LD, lipid droplet. D: Representative images of CTRL and ethanol hepatocytes showing detailed intracellular structures in the PP and PV areas. LD, lipid droplet; mit, mitochondria; gly, glycogen; RER, rough endoplasmic reticulum; bc, bile canaliculus; GC, fragmented Golgi complex; Dis, Space of Disse; EC, endothelial cell; SER, smooth endoplasmic reticulum; Nuc, nucleus; * collagen fibers. Bar scale = 400 nm. E: Mitochondrial area and length in livers quantified from images of

segregation in the functional capacity of mitochondria in basal conditions, determined most likely by the zoned spatial characteristics of the liver acinus. However, while these changes remained unchanged in PP from alcohol-fed mice, chronic alcohol intake reversed the decrease of respiratory parameters in PV hepatocytes (Fig. 7C) that were accompanied by an increase in mitochondrial mass as shown by higher levels of porin in PV hepatocytes from alcohol-fed mice (Fig. 7D). These findings indicate that chronic alcohol feeding stimulates mitochondrial respiration in PV hepatocytes.

Hepatocyte-specific *Stard1* deletion protects from alcohol-induced oxidative stress in PV hepatocytes

Given the preceding findings, we next explored the cause-and-effect relationship between increased StARD1 expression and alcohol-induced oxidative stress, focusing particularly in PV hepatocytes, which is the parenchymal population most sensitive to the oxidative stress and injury caused by alcohol intake. First, immunohistochemical analyses of liver sections stained with anti-StARD1 and anti-GLUL antibodies confirmed the predominant expression of StARD1 in PV zone of the liver in *Stard1*$^{f/f}$ mice fed alcohol (**Fig. 8**A). These findings paralleled the increased expression of StARD1 in PV hepatocytes isolated from *Stard1*$^{f/f}$ mice that was dampened in PV hepatocytes from *Stard1*$^{\Delta hep}$ mice fed alcohol (Fig. 8B). Consistent with these findings, alcohol caused a significant increase in mitochondrial cholesterol (Fig. 8C) and subsequent mGSH depletion (**Fig. 9**A) as well as oxidative stress reflected by increased levels of 4-HNE (Fig. 9B) in PV hepatocytes from *Stard1*$^{f/f}$ mice but not *Stard1*$^{\Delta hep}$ mice fed alcohol (Figs. 8C and 9A, B). Furthermore, hepatocyte-specific *Stard1* deletion protected against alcohol-induced liver injury reflected by the decrease in the release of serum transaminases (Fig. 9C) and alcohol-induced steatosis (Fig. 9D). Thus, these findings establish a crucial role for StARD1 as a causal mediator of alcohol-induced oxidative stress in PV hepatocytes.

Stard1 deletion attenuates the mitochondrial ultrastructural alterations caused by alcohol feeding

Besides the changes in oxidative stress, we next explored whether StARD1 deletion modulated the effects of alcohol intake in ultrastructure of intracellular organelles, including the mitochondria. Livers from *Stard1*$^{f/f}$ and *Stard1*$^{\Delta hep}$ fed alcohol or control diets were prepared for TEM analyses. Fixed livers were processed as described before and hepatocytes selected from PV areas were analyzed. **Figure 10** shows representative images of hepatocytes in the centrilobular zone (PV) revealing that specific hepatocyte StARD1 depletion significantly rescued the ultrastructural phenotype, in agreement with the biochemical data. In particular, the PV zone showed a marked increase in the content of glycogen of *Stard1*$^{\Delta hep}$ mice fed alcohol compared to *Stard1*$^{f/f}$ mice (Fig. 10A, B). Moreover, the number of LD tended to decrease in *Stard1*$^{\Delta hep}$ mice fed alcohol. (Fig. 10C). Besides, mitochondria from *Stard1*$^{\Delta hep}$ mice fed alcohol exhibited well-differentiated cristae and intact inner and outer mitochondrial membranes and electron dense matrix (see high magnification images Fig. 10A) with respect to *Stard1*$^{f/f}$ mice. Like in control hepatocytes, mitochondria appeared surrounded with RER, and only small, scattered regions with SER could be observed. Although *Stard1* deletion did not affect the number or length of mitochondria, it decreased the mitochondrial area determined from TEM images compared to *Stard1*$^{f/f}$ mice (Fig. 10D). Thus, these findings indicate a crucial role for StARD1 in determining the ultrastructure of intracellular components of PV hepatocytes, particularly mitochondria and ER.

DISCUSSION

Despite being one of the leading causes of chronic liver disease and mortality, the pathogenesis of ALD is still incompletely understood, which has limited the availability of effective therapies. The anatomical features and functional complexity of zone-restricted gene expression makes it even more challenging to understand the mechanisms whereby chronic alcohol intake injure hepatocytes and sensitize to disease progression. Here, we uncover a spatial distribution of the expression of StARD1 induced by alcohol metabolism in mice fed alcohol using chronic and acute-on-chronic models of ALD. In both cases we observe the predominant expression of StARD1 in the PV zone of the liver, coinciding with the area in which not only alcohol is preferentially metabolized by the inducible expression of CYP2E1 but also where most of the damaging effects of alcohol take place (34). Our findings in PMH revealed a synergism between alcohol and chemical hypoxia in increasing the expression of StARD1, which is not observed for CYP2E1, indicating the specificity of this synergism in the induction of StARD1 in PV hepatocytes. These findings are consistent with StARD1 expression being regulated by ER stress and hypoxia (18, 27, 42). Although we did not examine the

ultrathin sections and analyzed using ImageJ software. Data are presented as means ± SEM (N > 3, $P < 0.05$, Two-way ANOVA (B (diet: F = 120.4, $P < 0.001$; zonality: F = 19.42, $P < 0.001$; interaction F = 3.537, P = n.s.), C (diet: F = 37.76, $P < 0.001$; zonality: F = 10.14, $P < 0.05$; interaction F = 63.28, $P < 0.001$), (E) mitochondrial number (diet: F = 27.58, $P < 0.001$; zonality: F = 53.46, $P < 0.001$; interaction F = 0.106, P = n.s.) and (E) mitochondrial length (diet: F = 0.001, P = n.s.; zonality: F = 23.35, $P < 0.001$; interaction F = 1.183, P = n.s.)) followed by Tukey's multiple comparison test). F: Representative images of CTRL and ethanol, as indicated, at high magnification showing the ultrastructural morphology of mitochondria in PP and PV areas. Bar scale = 400 nm. PP, periportal; PV, perivenous; RER, rough endoplasmic reticulum; TEM, transmission electron microscope.

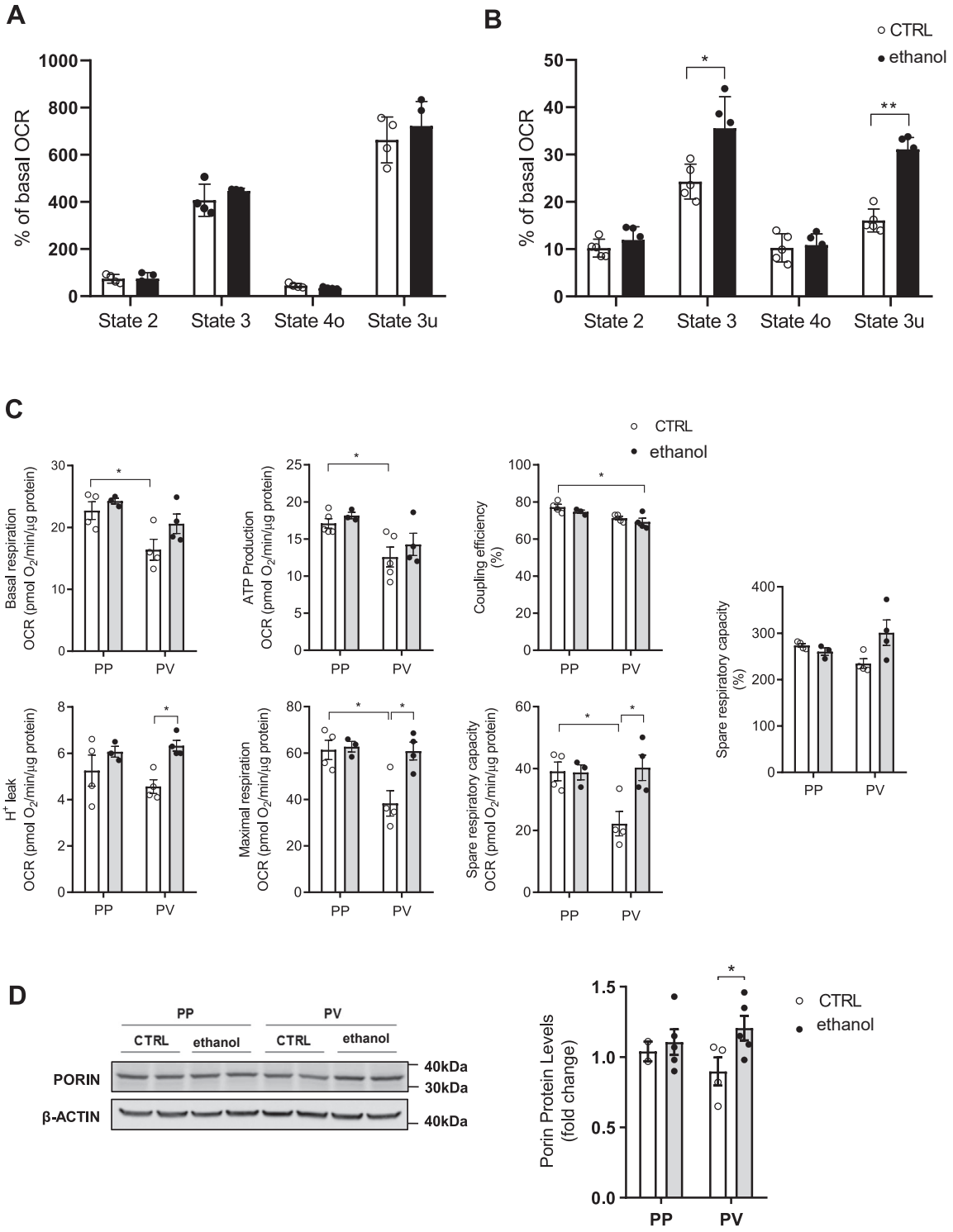

Fig. 7. Extracellular flux analysis of mitochondria and zonal hepatocytes from alcohol-fed mice. WT C57BL/6J mice were fed an alcohol diet for 30 days. A: Pyruvate and Malate-driven mitochondrial respiration. State 2: pyruvate and malate (10 mM), State 3: ADP (4 mM), State 4o: Oligomycin (2.5 µg/ml) and State 3u: FCCP (4 µM). B: Succinate (10 mM) and rotenone (2 µM) driven mitochondrial respiration in different states as in A. Data are presented as means ± SEM (N > 3, *$P < 0.05$, Unpaired Student's *t* test (two tailed)). C: Mitochondrial respiration flux profile with basal respiration, ATP-linked respiration, coupling efficiency, H+ leak, maximal respiration, and spare respiratory capacity of CTRL or ethanol PP and PV hepatocytes. D: Western blot of homogenates from isolated PP and PV hepatocytes showing the Porin protein expression levels (mitochondrial mass marker) and quantification by ImageJ software. Respiratory control ratios were normalized by total protein content. Data are presented as means ± SEM (N > 5, $P < 0.05$, Two-way ANOVA (C basal (diet: F = 3.723, P = n.s.; zonality: F = 11.27, $P < 0.01$; interaction F = 0.798, P = n.s.), (C) ATP (diet: F = 1.403, P = n.s.; zonality: F = 12.94, $P < 0.01$; interaction F = 0.074, P = n.s.), C Coupling (diet: F = 2.296, P = n.s.; zonality: F = 14.24, $P < 0.01$; interaction F = 0.037, P = n.s.), C H^+ (diet: F = 9.031, $P < 0.05$; zonality: F = 0.252, P = n.s.; interaction F = 1.222, P = n.s.), C Maximal

expression of ER stress markers, ER stress is a well-known player in the progression of ALD (2, 3, 5, 61). Whether alcohol-induced ER stress is spatially distributed in the liver remains to be further investigated in detail. Hypoxia, however, is an intrinsic factor of the PV area of the acinus determined largely by the anatomical features of oxygen flow from the portal to the central vein that can contribute in part to the segregation of zone-specific functions of the liver (30, 31). Besides this anatomical feature, chronic alcohol intake is known to increase hepatic oxygen consumption, which can further contribute to the pericentral hypoxia in the liver (62, 63), consistent with our findings showing enhanced pimonidazole staining in colocalization with GLUL in liver sections from alcohol-fed mice.

StARD1 is the founding member of an expanding family of proteins with lipid-binding pocket domains, which encompasses other members that have been shown to mediate intracellular cholesterol trafficking. In this regard, the role of StARD3 in delivering cholesterol to mitochondria has been documented in various contexts, including lysosomal storage disorders like Niemann-Pick type C disease (64). However, unlike StARD1, the hepatic expression of StARD3 did not change in chronic alcohol-fed mice, indicating that the inducing effect of alcohol was specific for StARD1, which lends further support for the contribution of this particular member of the StAR family in the delivery of cholesterol to the mitochondria in the context of ALD. In line with the known function of StARD1, chronic alcohol intake resulted in a predominant accumulation of cholesterol in the mitochondria from PV hepatocytes that translated in a significant depletion of mitochondrial GSH defense and increased oxidative stress and lipid peroxidation. Thus, although previous findings demonstrated an increased expression of StARD1 in alcohol-fed mice and patients with ALD (18), the current findings significantly extend these observations linking the expression of StARD1 with the onset of oxidative stress and lipid peroxidation in a zone-specific fashion, namely the pericentral zone, which is endowed with the greatest capacity to metabolize alcohol while exhibiting the lowest antioxidant defense reflected by decreased mitochondrial GSH content determined by increased mitochondrial cholesterol loading.

As StARD1-mediated delivery of cholesterol to mitochondria is the rate-limiting step in the generation of 27-hydroxycholesterol, which serves as a precursor for BA synthesis in the alternative pathway (43–46), it could be anticipated that alcohol-induced StARD1 expression may result in an increased BAs content in a zone-dependent manner, mirroring the expression of StARD1. Intriguingly, however, BAs levels in liver extracts from alcohol-fed mice did not change with respect to control mice, being similar between PP and PV hepatocytes. Besides the increase in StARD1 in PV area, the expression of the enzymes involved in the synthesis of BAs in the acidic mitochondrial pathway was lower in alcohol-fed mice, in line with previous reports (49–51). Thus, although our findings do not support a role for chronic alcohol consumption in the onset of cholestasis and contrast with the increase of serum BAs in patients with ALD (48), further investigation will be required to estimate whether other models of ALD that elicit a more severe pathology, e.g., intragastric model, have an impact in the synthesis of BAs and the specific contribution of the alternative mitochondrial pathway.

TEM analyses indicated important morphological spatial changes following alcohol intake, including a drastic decrease in the glycogen content that was more predominant in the PV zone, consistent with previous findings in patients with ALD (52), and an increased homogeneous population of LD in the same zone. These changes were also accompanied by a fragmentation of the Golgi in PP hepatocytes as reported previously (65, 66) and a marked increase in the tubular SER in the PV zone, likely to accommodate the inducible expression of cytochromes, particularly CYP2E1, to metabolize alcohol (55–57). In line with the contribution of the disruption of mitochondrial dynamics in the progression of ALD (67, 68), chronic alcohol feeding also resulted in a zone-dependent morphological change in the shape and number of mitochondria. Interestingly, the length of mitochondria in the PV area was reduced compared to the PP zone and although alcohol intake did not significantly impact this feature it did result in an increase in mitochondrial number. Remarkably, hepatocyte-specific deletion of *Stard1* reversed these structural alterations caused by alcohol consumption, not only regarding mitochondrial ultrastructure, which exhibited preserved cristae and mitochondrial membranes and a reduced area, but also related to the changes in SER and glycogen content. As the regulation of liver architecture controls metabolic homeostasis in the context of obesity (69), the impact of StARD1 in hepatocyte ultrastructure suggests that StARD1 could emerge as a regulator of liver metabolism in ALD. These changes translated in alterations in mitochondrial function monitored by OCR, with an increased complex II-driven mitochondrial respiration from alcohol-fed mice, consistent with reports showing that chronic alcohol intake results in the stimulation of mitochondrial respiration and a higher complex II

(diet: F = 7.430, $P < 0.05$; zonality: F = 8.033, $P < 0.05$; interaction F = 5.844, $P < 0.05$), C spare (diet: F = 6.040, $P < 0.05$; zonality: F = 4.520, P = n.s.; interaction F = 6.466, $P < 0.05$), C spare % (diet: F = 2.615, P = n.s.; zonality: F = 0.002, P = n.s.; interaction F = 5.945, $P < 0.05$) and D (diet: F = 3.256, P = n.s.; zonality: F = 0.042, P = n.s.; interaction F = 1.365, P = n.s.)) followed by Tukey's multiple comparison test. FCCP, carbonyl cyanide 4-(trifluoromethoxy) phenylhydrazone; OCR, oxygen consumption rate; PP, periportal; PV, perivenous.

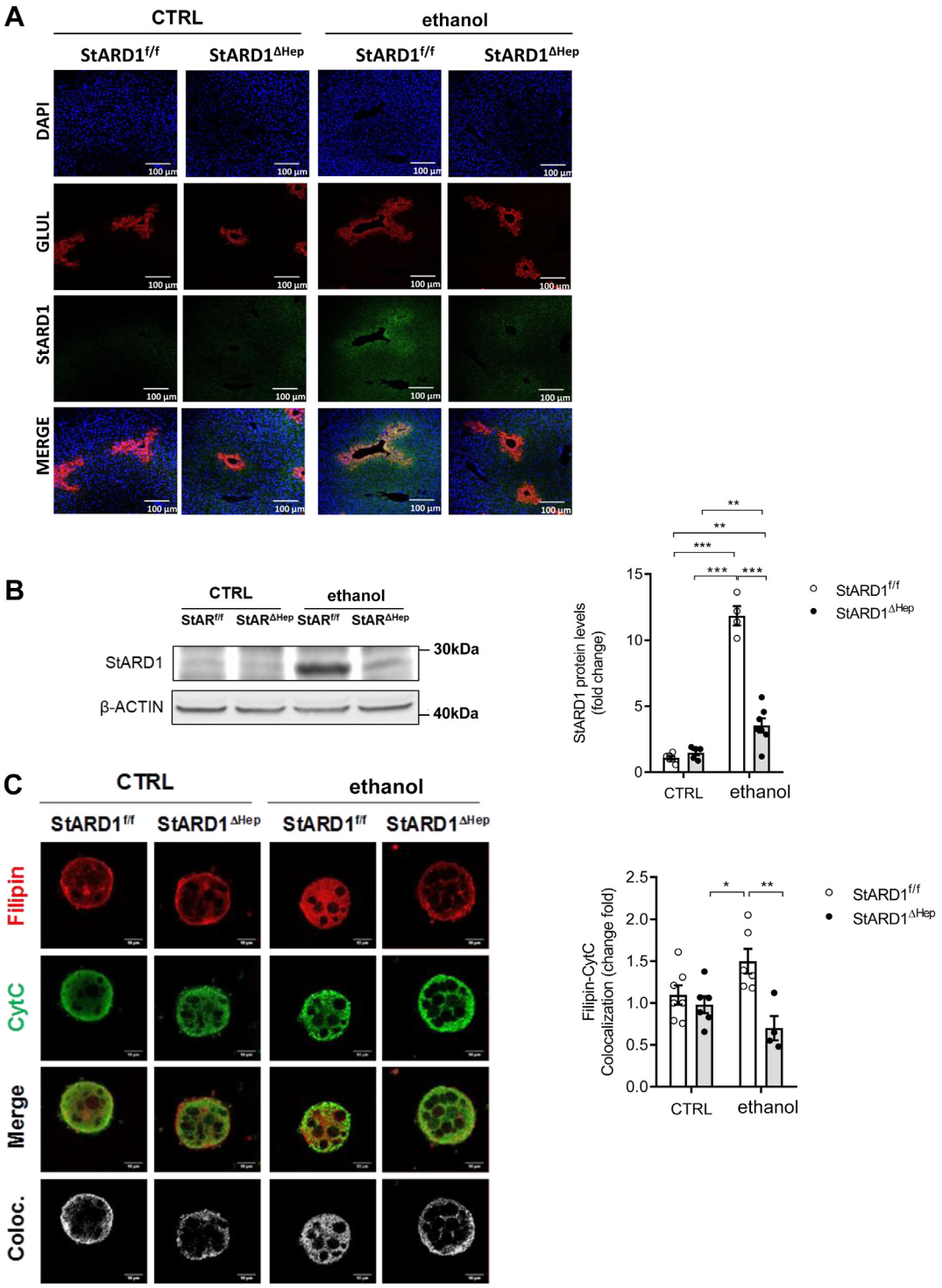

Fig. 8. Hepatocyte-specific *Stard1* deletion prevents alcohol-induced mitochondrial cholesterol accumulation and oxidative stress in PV hepatocytes. A: Characterization of subcellular localization of GLUL and StARD1 in mouse liver. Representative immunohistofluorescence images from at least 3 replicates per group at 10 days after ethanol feeding. Bar scale = 100 μm. B: Western blot of homogenates from isolated PV hepatocytes showing protein levels of StARD1 and protein expression quantification by ImageJ software. C: Mitochondrial cholesterol levels were analyzed in PV hepatocytes by immunocytochemistry using anti-CytC and Filipin. Bar scale = 10 µm. Staining markers colocalization was analyzed using ImageJ software. Values are the mean ± SEM of >6 animals per group. $P < 0.05$. Two-way ANOVA (A (diet: F = 2.744 P = n.s.; phenotype: F = 12.81, $P < 0.01$; interaction F = 3.586, P = n.s.) and C (diet: F = 12.49, $P < 0.01$; phenotype: F = 0.221, P = n.s.; interaction F = 6.942, $P < 0.05$)) followed by Tukey's multiple comparison test. GLUL, glutamine synthase; PV, perivenous; StARD1, steroidogenic acute regulatory protein.

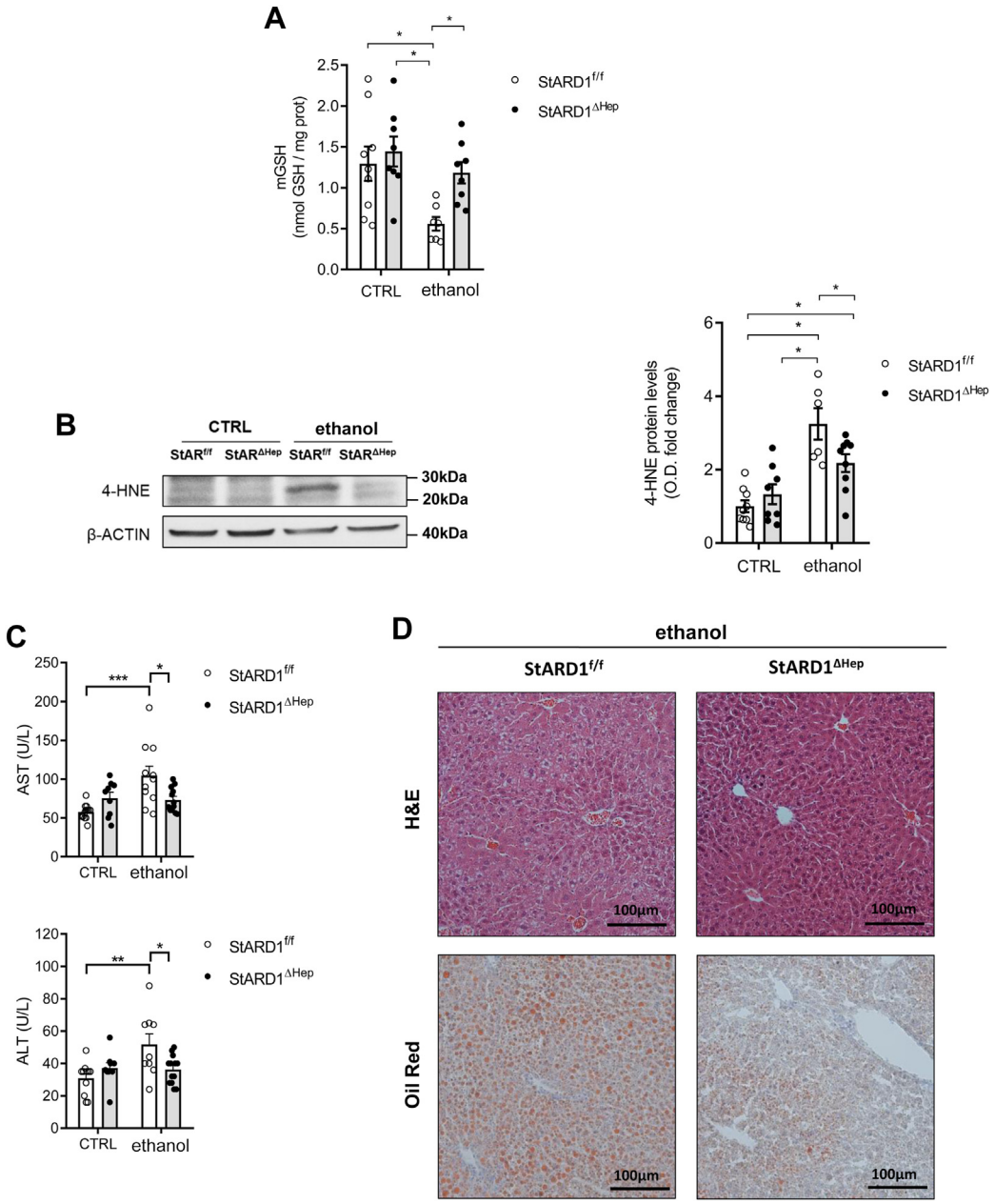

Fig. 9. Hepatocyte-specific Stard1 deletion protects against alcohol-induced oxidative stress in PV zone. A: GSH levels in CTRL or ethanol PV hepatocytes from StARD1$^{f/f}$ and StARD1$^{\Delta Hep}$ mice. B: 4-HNE protein levels from StARD1$^{f/f}$ and StARD1$^{\Delta Hep}$ CTRL or ethanol PV hepatocytes. C: Serum AST and ALT levels from CTRL and ethanol mice. D: Liver sections of ethanol-fed StARD1$^{f/f}$ and StARD1$^{\Delta Hep}$ mice analyzed by H&E and Oil red staining. Bar scale = 100 µm. Values are the mean ± SEM of >6 animals per group. $P < 0.05$. Two-way ANOVA (A) (diet: F = 5.241, $P < 0.05$; phenotype: F = 8.717, $P < 0.01$; interaction F = 1.975, P = n.s.), (B) (diet: F = 1.868, P = n.s.; phenotype: F = 32.93, $P < 0.001$; interaction F = 6.677, $P < 0.05$), (C) AST: (diet: F = 14.66, $P < 0.01$; phenotype: F = 1.347, P = n.s.; interaction F = 17.97, $P < 0.01$) and (C) ALT: (diet: F = 12.37, $P < 0.05$; phenotype: F = 2.670, P = n.s.; interaction F = 14.66, $P < 0.01$) followed by Tukey's multiple comparison test. 4-HNE, 4-hydroxynonenal; ALT, alanine aminotransferase; AST, aspartate aminotransferase; PV, perivenous; StARD1, steroidogenic acute regulatory protein.

relative to complex I-driven OCR (58–60). Interestingly, OCR determination in control mice revealed a significant depression of mitochondrial respiration in PV compared to PP hepatocytes, likely reflecting the change in mitochondrial length that was not compensated by the insufficient mitochondrial number. However, these determinations in alcohol-fed mice revealed the stimulation of mitochondrial respiratory parameters, including maximal respiration and increased spared respiratory capacity in PV hepatocytes from alcohol-fed mice compared to control mice, suggesting that the increased mitochondrial number in this population compensates for the effect of alcohol in mitochondrial length. An intriguing aspect is the stimulation of mitochondrial respiration by alcohol feeding despite accumulation of cholesterol in mitochondria. While individual mitochondrial with increased cholesterol may respire less efficiently (21), it is conceivable that an

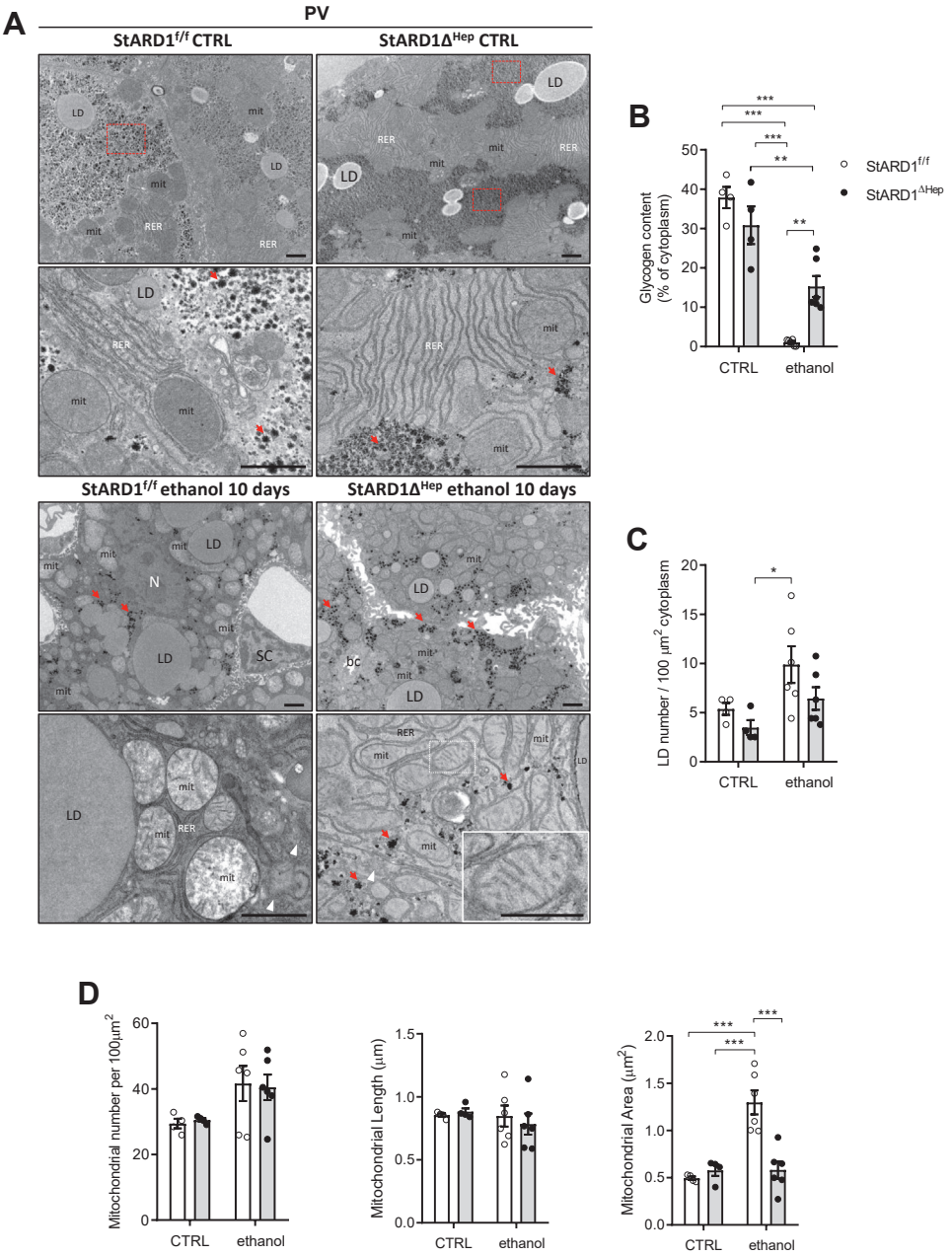

Fig. 10. Ultrastructural analysis of PV area in *Stard1* deleted hepatocytes of alcohol-fed mice. StARD1$^{f/f}$ and StARD1$^{\Delta Hep}$ were fed with chow or alcohol diet for 10 days and livers perfused and processed for conventional TEM. Ultrathin sections were analyzed and representative images from the PV area, at two different magnifications, from 3 livers examined (A) and quantified (B–D). Control livers, with chow diet (StARD1$^{f/f}$, upper panels) showed the normal architecture and compartments also observed in Figure 6. This is indicative that genetic models StARD1$^{f/f}$ or StARD1$^{\Delta Hep}$ were not affected and the ultrastructure of the liver parenchyma was largely intact. Large accumulation of glycogen is evident (see red dashed squares) and scattered small red arrows in high magnification images together with large amount of tubular RER and mitochondria. Panels below showed details of PV hepatocytes from livers of mice fed with alcohol diet for 10 days. Compared to controls, StARD1$^{f/f}$ livers showed a drastic reduction of glycogen (B) and slightly increased of LD (C). The number and length of mitochondria were similar to controls (D). Strikingly, the deletion of StARD1 in alcohol-fed mice impact the morphology of hepatocytes reflected by a significant increase in glycogen (small red arrows point scattered rosettes of glycogen) (B); changes in mitochondria ultrastructure with well-differentiated cristae, electron density matrix, and decreased area (D) compared to StARD1$^{f/f}$ hepatocytes (scale bar insets = 500 nm). LD, lipid droplet; mit, mitochondria; RER, rough endoplasmic reticulum; SER, smooth endoplasmic reticulum; bc, bile canaliculus; Dis, Space of Disse; EC, Endothelial cell; SC, stellate cell; N, Nucleus. Bar scale = 1 μm. Quantifications were performed with ImageJ as in Figure 6. Data are presented as means ± SEM (N > 3, $P < 0.05$, Two-way ANOVA (B (diet: F = 71.96, $P < 0.001$; phenotype: F = 1.354, P = n. s.; interaction F = 11.83, $P < 0.01$), (C) (diet: F = 25.20, $P < 0.05$; phenotype: F = 12.96, P = n. s.; interaction F = 1.090, P = n. s.), (D) Mitochondrial number per 100 µm : (diet: F = 30.37, $P < 0.05$; phenotype: F = 0.001, P = n.s.; interaction F = 0.324, P = n. s.) and (D) Mitochondrial length: (diet: F = 2.937, P = n.s.; phenotype: F = 0.337, P = n.s.; interaction F = 2.143, P = n.s.) followed by Tukey's multiple comparison test. LD, lipid droplet; PV, perivenous; RER, rough endoplasmic reticulum; StARD1, steroidogenic acute regulatory protein; TEM, transmission electron microscope.

increased population of poorly respiring mitochondria may result in a net increase in oxygen consumption, which will require further investigation in the future. The question is how to link the stimulation in mitochondrial respiration with the area being most sensitive to alcohol-induced damage like PV. While challenging, this issue may relate to recent findings correlating increased mitochondrial respiration in mice fed alcohol with liver injury and advanced ALD pathology (58, 59), in which the stimulated oxygen consumption in the mitochondrial electron transport chain was linked to a more effective regeneration of NAD^+ from NADH to accelerate alcohol metabolism. A derived consequence of the increased mitochondrial respiration would be expected to generate more ROS, which can contribute to the predominant zonal damage in ALD.

In summary, our current findings identify an additional factor that can contribute to the spatial, zonal-dependent sensitivity of the liver to the damaging effects of alcohol besides the known preferential metabolism of alcohol in the centrilobular area. Several factors converge in this area, such as lower oxygen tension and alcohol metabolism that synergize to induce StARD1, leading to subsequent mitochondrial cholesterol delivery that disrupts mitochondrial antioxidant defense and function, suggesting that targeting StARD1 may be a novel approach for ALD.

Data availability

All data that support the findings are included in the manuscript and supporting information.

Supplemental data

This article contains supplemental data.

Acknowledgments

We want to thank Eva Prats, Josep Manel Rebled, Rosa Rivera, Mora Gimeno, and Adriana Martínez from Transmission electron microscopy unit (TEM) for technical support. Carmen Garcia-Ruiz and Jose C Fernandez-Checa belong to the Spanish National Research Council's Cancer Hub. We acknowledge the support from grants PID2019-111669RB-I00 and PID2020-115055RB-I00 from Plan Nacional de I+D funded by the Agencia Estatal de Investigación (AEI) and the Fondo Europeo de Desarrollo Regional (FEDER) and from the CIBEREHD; the center grant P50AA011999 Southern California Research Center for ALPD and Cirrhosis funded by NIAAA/NIH; as well as support from AGAUR of the Generalitat de Catalunya SGR-2017-1112, European Cooperation in Science & Technology (COST) ACTION CA17112, Prospective European Drug-Induced Liver Injury Network, the 2018-102799-T "Enfermedades Metabólicas y Cancer" from the Red Nacional of the Spanish Health Ministry and the Project 201916/31 Contribution of mitochondrial oxysterol and bile acid metabolism to liver carcinogenesis 2019 by Fundació Marató TV3, and the COVID grant from the Spanish Association for the Study of the Liver (AEEH). In addition, this project has received funding from the European Horizon's research and innovation program HORIZON-HLTH-2022-STAYHLTH-02 under agreement No 101095679.

Author contributions

R. F., C. G.-R., and J. C. F.-C. conceptualization; R. F., E. S.-V., S. T., S. N., N. I.-U., A. E., M. C., A. B., G. M., C. G.-R., and J. C. F.-C. methodology; R. F., E. S.-V., S. T., C. E., C. G.-R., and J. C. F.-C. investigation; R. F., E. S.-V, S. T., C. E., C. G.-R., and J. C. F.-C. writing; R. F., E. S.-V, S. T., C. E., C. G.-R, and J. C. F.-C. visualization; C. G.-R and J. C. F.-C. supervision; C. G.-R and J. C. F.-C. project administration; C. G.-R and J. C. F.-C. funding acquisition.

Author ORCIDs

Raquel Fucho https://orcid.org/0000-0002-1774-9099
Estel Solsona-Vilarrasa https://orcid.org/0000-0001-9774-8055
Sandra Torres https://orcid.org/0000-0002-2894-3188
Albert Edo https://orcid.org/0000-0003-3951-524X
Carmen García-Ruiz https://orcid.org/0000-0002-2652-6102
Jose C. Fernandez-Checa https://orcid.org/0000-0003-3422-2990

Funding and additional information

R. F. was funded by "Juan de la Cierva Incorporación" from the National Programme for the Promotion of Talent and Its Employability of the "Ministerio de Ciencia, Innovación y Universidades" (IJCI-2015-23219) of the Spanish Government. E. S.-V. was supported by a contract from the "Ministerio de Educación, Cultura y Deporte" (FPU15/04537) of the Spanish Government. Its contents are solely the responsibility of the authors and do not necessarily represent the official views of the National Institutes of Health.

Conflict of interest

The authors declare they have no conflict of interest with the contents of this article.

Abbreviations

ALD, alcoholic-related liver disease; ALDH, acetaldehyde dehydrogenase; ER, endoplasmic reticulum; GLUL, glutamine synthase; GST-PFO, glutathione-S-transferase tag fused with the perfringolysin O; HIF, hypoxia-inducible factor; HNE, hydroxynonenal; LDs, lipid droplets; OCR, oxygen consumption rates; PMH, primary mouse hepatocytes; PP, periportal; PV, perivenous; RER, rough endoplasmic reticulum; ROS, reactive oxygen species; SER, smooth endoplasmic reticulum; StARD1, steroidogenic acute regulatory protein; TEM, transmission electron microscope.

Manuscript received March 23, 2023, and in revised form June 26, 2023. Published, JLR Papers in Press, July 19, 2023, https://doi.org/10.1016/j.jlr.2023.100413

REFERENCES

1. Louvet, A., and Mathurin, P. (2015) Alcoholic liver disease: mechanisms of injury and targeted treatment. *Nat. Rev. Gastroenterol. Hepatol.* **12**, 231–242

2. Hernandez-Tejero, M., Clemente-Sanchez, A., and Bataller, R. (2023) Spectrum, screening, and diagnosis of alcohol-related liver disease. *J. Clin. Exp. Hepatol.* **13**, 75–87
3. Gao, B., and Bataller, R. (2011) Alcoholic liver disease: pathogenesis and new therapeutic targets. *Gastroenterology.* **141**, 1572–1585
4. Cederbaum, A. I. (2012) Alcohol metabolism. *Clin. Liver Dis.* **16**, 667
5. Osna, N. A., Rasineni, K., Ganesan, M., Donohue, T. M., and Kharbanda, K. K. (2022) Pathogenesis of alcohol-associated liver disease. *J. Clin. Exp. Hepatol.* **12**, 1492–1513
6. García-Ruiz, C., and Fernández-Checa, J. C. (2018) Mitochondrial oxidative stress and antioxidants balance in fatty liver disease. *Hepatol. Commun.* **2**, 1425–1439
7. Ohashi, K., Pimienta, M., and Seki, E. (2018) Alcoholic liver disease: a current molecular and clinical perspective. *Liver Res.* **2**, 161–172
8. Lieber, C. S. (2005) Metabolism of alcohol. *Clin. Liver Dis.* **9**, 1–35
9. Jeon, S., and Carr, R. (2020) Alcohol effects on hepatic lipid metabolism. *J. Lipid Res.* **61**, 470
10. Krishnasamy, Y., Ramshesh, V. K., Gooz, M., Schnellmann, R. G., Lemasters, J. J., and Zhong, Z. (2016) Ethanol and high cholesterol diet causes severe steatohepatitis and early liver fibrosis in mice. *PLoS One.* **11**, e0163342
11. Zhong, S., Li, L., Liang, N., Zhang, L., Xu, X., Chen, S., *et al.* (2021) Acetaldehyde dehydrogenase 2 regulates HMG-CoA reductase stability and cholesterol synthesis in the liver. *Redox Biol.* **41**, 101919
12. Vance, J. E. (2014) MAM (mitochondria-associated membranes) in mammalian cells: lipids and beyond. *Biochim. Biophys. Acta.* **1841**, 595–609
13. Tatsuta, T., Scharwey, M., and Langer, T. (2014) Mitochondrial lipid trafficking. *Trends Cell Biol.* **24**, 44–52
14. Varatharajalu, R., Garige, M., Leckey, L. C., Arellanes-Robledo, J., Reyes-Gordillo, K., Shah, R., *et al.* (2014) Adverse signaling of scavenger receptor class B1 and PGCIs in alcoholic hepatosteatosis and steatohepatitis and protection by betaine in rat. *Am. J. Pathol.* **184**, 2035–2044
15. Zhao, P., and Slattery, J. T. (2002) Effects of ethanol dose and ethanol withdrawal on rat liver mitochondrial glutathione: implication of potentiated acetaminophen toxicity in alcoholics. *Drug Metab. Dispos.* **30**, 1413–1417
16. Zhao, P., Kalhorn, T. F., and Slattery, J. T. (2002) Selective mitochondrial glutathione depletion by ethanol enhances acetaminophen toxicity in rat liver. *Hepatology.* **36**, 326–335
17. Marí, M., Morales, A., Colell, A., García-Ruiz, C., and Fernández-Checa, J. C. (2014) Mitochondrial cholesterol accumulation in alcoholic liver disease: role of ASMase and endoplasmic reticulum stress. *Redox Biol.* **3**, 100
18. Fernandez, A., Matias, N., Fucho, R., Ribas, V., Von Montfort, C., Nuño, N., *et al.* (2013) ASMase is required for chronic alcohol induced hepatic endoplasmic reticulum stress and mitochondrial cholesterol loading. *J. Hepatol.* **59**, 805–813
19. Marí, M., Caballero, F., Colell, A., Morales, A., Caballeria, J., Fernandez, A., *et al.* (2006) Mitochondrial free cholesterol loading sensitizes to TNF- and Fas-mediated steatohepatitis. *Cell Metab.* **4**, 185–198
20. Colell, A., García-Ruiz, C., Miranda, M., Ardite, E., Marí, M., Morales, A., *et al.* (1998) Selective glutathione depletion of mitochondria by ethanol sensitizes hepatocytes to tumor necrosis factor. *Gastroenterology.* **115**, 1541–1551
21. Solsona-Vilarrasa, E., Fucho, R., Torres, S., Nuñez, S., Nuño-Lámbarri, N., Enrich, C., *et al.* (2019) Cholesterol enrichment in liver mitochondria impairs oxidative phosphorylation and disrupts the assembly of respiratory supercomplexes. *Redox Biol.* **24**, 101214
22. García-Ruiz, C., Kaplowitz, N., and Fernandez-Checa, J. C. (2013) Role of mitochondria in alcoholic liver disease. *Curr. Pathobiol. Rep.* **1**, 159–168
23. Fromenty, B., Grimbert, S., Mansouri, A., Beaugrand, M., Erlinger, S., Rötig, A., *et al.* (1995) Hepatic mitochondrial DNA deletion in alcoholics: association with microvesicular steatosis. *Gastroenterology.* **108**, 193–200
24. Goicoechea, L., Conde de la Rosa, L., Torres, S., García-Ruiz, C., and Fernández-Checa, J. C. (2023) Mitochondrial cholesterol: metabolism and impact on redox biology and disease. *Redox Biol.* **61**, 102643
25. Stocco, D. M. (2001) StAR protein and the regulation of steroid hormone biosynthesis. *Annu. Rev. Physiol.* **63**, 193–213
26. Larsen, M. C., Lee, J., Jorgensen, J. S., and Jefcoate, C. R. (2020) STARD1 functions in mitochondrial cholesterol metabolism and Nascent HDL formation. Gene expression and molecular mRNA imaging show novel splicing and a 1:1 mitochondrial association. *Front Endocrinol. (Lausanne).* **11**, 559674
27. Torres, S., Baulies, A., Insausti-Urkia, N., Alarcón-Vila, C., Fucho, R., Solsona-Vilarrasa, E., *et al.* (2019) Endoplasmic reticulum stress-induced upregulation of STARD1 promotes acetaminophen-induced acute liver failure. *Gastroenterology.* **157**, 552–568
28. Conde de la Rosa, L., Garcia-Ruiz, C., Vallejo, C., Baulies, A., Nuñez, S., Monte, M. J., *et al.* (2021) STARD1 promotes NASH-driven HCC by sustaining the generation of bile acids through the alternative mitochondrial pathway. *J. Hepatol.* **74**, 1429–1441
29. Ben-Moshe, S., and Itzkovitz, S. (2019) Spatial heterogeneity in the mammalian liver. *Nat. Rev. Gastroenterol. Hepatol.* **16**, 395–410
30. Kietzmann, T. (2017) Metabolic zonation of the liver: the oxygen gradient revisited. *Redox Biol.* **11**, 622–630
31. Jungermann, K., and Kietzmann, T. (1996) Zonation of parenchymal and nonparenchymal metabolism in liver. *Annu. Rev. Nutr.* **16**, 179–203
32. Bühler, R., Lindros, K. O., Nordling, Å., Johansson, I., and Ingelman-Sundberg, M. (1992) Zonation of cytochrome P450 isozyme expression and induction in rat liver. *Eur. J. Biochem.* **204**, 407–412
33. Dicker, E., and Cederbaum, A. I. (1991) Increased oxidation of dimethylnitrosamine in pericentral microsomes after pyrazole induction of cytochrome P-4502E1. *Alcohol Clin. Exp. Res.* **15**, 1072–1076
34. Popper, H., and Leiber, C. S. (1980) Histogenesis of alcoholic fibrosis and cirrhosis in the baboon. *Am. J. Pathol.* **98**, 695
35. García-Ruiz, C., Morales, A., Ballesta, A., Rodés, J., Kaplowitz, N., and Fernández-Checa, J. C. (1994) Effect of chronic ethanol feeding on glutathione and functional integrity of mitochondria in periportal and perivenous rat hepatocytes. *J. Clin. Invest.* **94**, 193–201
36. García-Ruiz, C., Morales, A., Colell, A., Ballesta, A., Rodés, J., Kaplowitz, N., *et al.* (1995) Feeding S-adenosyl-L-methionine attenuates both ethanol-induced depletion of mitochondrial glutathione and mitochondrial dysfunction in periportal and perivenous rat hepatocytes. *Hepatology.* **21**, 207–214
37. Bertola, A., Mathews, S., Ki, S. H., Wang, H., and Gao, B. (2013) Mouse model of chronic and binge ethanol feeding (the NIAAA model). *Nat. Protoc.* **8**, 627–637
38. Alarcón-Vila, C., Insausti-Urkia, N., Torres, S., Segalés-Rovira, P., Conde de la Rosa, L., Nuñez, S., *et al.* (2023) Dietary and genetic disruption of hepatic methionine metabolism induce acid sphingomyelinase to promote steatohepatitis. *Redox Biol.* **59**, 102596
39. Baulies, A., Montero, J., Matías, N., Insausti, N., Terrones, O., Basañez, G., *et al.* (2018) The 2-oxoglutarate carrier promotes liver cancer by sustaining mitochondrial GSH despite cholesterol loading. *Redox Biol.* **14**, 164
40. Goicoechea, L., Arenas, F., Castro, F., Nuñez, S., Torres, S., Garcia-Ruiz, C., *et al.* (2021) GST-perfringolysin O production for the localization and quantification of membrane cholesterol in human and mouse brain and liver. *STAR Protoc.* **3**, 101068
41. Tietze, F. (1969) Enzymic method for quantitative determination of nanogram amounts of total and oxidized glutathione: applications to mammalian blood and other tissues. *Anal. Biochem.* **27**, 502–522
42. Pandak, W. M., Ren, S., Marques, D., Hall, E., Redford, K., Mallonee, D., *et al.* (2002) Transport of cholesterol into mitochondria is rate-limiting for bile acid synthesis via the alternative pathway in primary rat hepatocytes. *J. Biol. Chem.* **277**, 48158–48164
43. Pandak, W. M., and Kakiyama, G. (2019) The acidic pathway of bile acid synthesis: not just an alternative pathway☆. *Liver Res.* **3**, 88–98
44. Ren, S., Hylemon, P. B., Marques, D., Gurley, E., Bodhan, P., Hall, E., *et al.* (2004) Overexpression of cholesterol transporter StAR increases in vivo rates of bile acid synthesis in the rat and mouse. *Hepatology.* **40**, 910–917
45. Kakiyama, G., Marques, D., Takei, H., Nittono, H., Erickson, S., Fuchs, M., *et al.* (2019) Mitochondrial oxysterol biosynthetic

pathway gives evidence for CYP7B1 as controller of regulatory oxysterols. *J. Steroid Biochem. Mol. Biol.* **189**, 36–47
46. Kowalewski, M. P., Gram, A., and Boos, A. (2015) The role of hypoxia and HIF1α in the regulation of STAR-mediated steroidogenesis in granulosa cells. *Mol. Cell. Endocrinol.* **401**, 35–44
47. Lefhvre, A. F., Decarli, L. M., and Lieber, C. S. (1972) Effect of ethanol on cholesterol and bile acid metabolism. *J. Lipid Res.* **13**, 48–55
48. Brandl, K., Hartmann, P., Jih, L. J., Pizzo, D. P., Argemi, J., Ventura-Cots, M., *et al.* (2018) Dysregulation of serum bile acids and FGF19 in alcoholic hepatitis. *J. Hepatol.* **69**, 396–405
49. Manley, S., and Ding, W. (2015) Role of farnesoid X receptor and bile acids in alcoholic liver disease. *Acta Pharm. Sin. B.* **5**, 158–167
50. Liu, Y., Liu, T., Zhao, X., and Gao, Y. (2022) New insights into the bile acid-based regulatory mechanisms and therapeutic perspectives in alcohol-related liver disease. *Cell. Mol. Life Sci.* **79**, 486
51. Fan, M., Wang, Y., Jin, L., Fang, Z., Peng, J., Tu, J., *et al.* (2022) Bile acid-mediated activation of Brown Fat protects from alcohol-induced steatosis and liver injury in mice. *Cell. Mol. Gastroenterol. Hepatol.* **13**, 809–826
52. Krähenbühl, L., Lang, C., Lüdes, S., Seiler, C., Schäfer, M., Zimmermann, A., *et al.* (2003) Reduced hepatic glycogen stores in patients with liver cirrhosis. *Liver Int.* **23**, 101–109
53. Bruguera, M., Bertran, A., Bombi, J. A., and Rodes, J. (1977) Giant mitochondria in hepatocytes. A diagnostic hint for alcoholic liver disease. *Gastroenterology.* **73**, 1383–1387
54. Williams, J. A., and Ding, W. X. (2015) Mitophagy, mitochondrial spheroids, and mitochondrial-derived vesicles in alcohol-induced liver injury. *Am. J. Physiol. Gastrointest. Liver Physiol.* **309**, G515
55. Remmer, H., and Merker, H. J. (1963) Drug-induced changes in the liver endoplasmic reticulum: association with drug-metabolizing enzymes. *Science.* **142**, 1657–1658
56. Park, J. W., Reed, J. R., Brignac-Huber, L. M., and Backes, W. L. (2014) Cytochrome P450 system proteins reside in different regions of the endoplasmic reticulum. *Biochem. J.* **464**, 241–249
57. Brignac-Huber, L. M., Park, J. W., Reed, J. R., and Backes, W. L. (2016) Cytochrome P450 organization and function are modulated by endoplasmic reticulum phospholipid heterogeneity. *Drug Metab. Dispos.* **44**, 1859–1866
58. Han, D., Johnson, H. S., Rao, M. P., Martin, G., Sancheti, H., Silkwood, K. H., *et al.* (2017) Mitochondrial remodeling in the liver following chronic alcohol feeding to rats. *Free Radic. Biol. Med.* **102**, 100–110
59. Han, D., Ybanez, M. D., Johnson, H. S., McDonald, J. N., Mesropyan, L., Sancheti, H., *et al.* (2012) Dynamic adaptation of liver mitochondria to chronic alcohol feeding in mice: biogenesis, remodeling, and functional alterations. *J. Biol. Chem.* **287**, 42165–42179
60. Goikoetxea-Usandizaga, N., Bravo, M., Egia-Mendikute, L., Abecia, L., Serrano-Maciá, M., Urdinguio, R. G., *et al.* (2023) The outcome of boosting mitochondrial activity in alcohol-associated liver disease is organ-dependent. *Hepatology.* https://doi.org/10.1097/HEP.0000000000000303
61. Ji, C., and Kaplowitz, N. (2004) Hyperhomocysteinemia, endoplasmic reticulum stress, and alcoholic liver injury. *World J. Gastroenterol.* **10**, 1699–1708
62. Arteel, G. E., Iimuro, Y., Yin, M., Raleigh, J. A., and Thurman, R. G. (1997) Chronic enteral ethanol treatment causes hypoxia in rat liver tissue in vivo. *Hepatology.* **25**, 920–926
63. Zelickson, B. R., Benavides, G. A., Johnson, M. S., Chacko, B. K., Venkatraman, A., Landar, A., *et al.* (2011) Nitric oxide and hypoxia exacerbate alcohol-induced mitochondrial dysfunction in hepatocytes. *Biochim. Biophys. Acta.* **1807**, 1573–1582
64. Balboa, E., Castro, J., Pinochet, M. J., Cancino, G. I., Matías, N., José Sáez, P., *et al.* (2017) MLN64 induces mitochondrial dysfunction associated with increased mitochondrial cholesterol content. *Redox Biol.* **12**, 274–284
65. Casey, C. A., Bhat, G., Holzapfel, M. S., and Petrosyan, A. (2016) Study of ethanol-induced Golgi disorganization reveals the potential mechanism of alcohol-impaired N-glycosylation. *Alcohol Clin. Exp. Res.* **40**, 2573–2590
66. Petrosyan, A. (2015) Onco-Golgi: is fragmentation a gate to cancer progression? *Biochem. Mol. Biol. J.* **1**, 16
67. Palma, E., Ma, X., Riva, A., Iansante, V., Dhawan, A., Wang, S., *et al.* (2019) Dynamin-1-like protein inhibition drives mega-mitochondria formation as an adaptive response in alcohol-induced hepatotoxicity. *Am. J. Pathol.* **189**, 580–589
68. Palma, E., Riva, A., Moreno, C., Odena, G., Mudan, S., Manyakin, N., *et al.* (2020) Perturbations in mitochondrial dynamics are closely involved in the progression of alcoholic liver disease. *Alcohol Clin. Exp. Res.* **44**, 856–865
69. Parlakgül, G., Arruda, A. P., Pang, S., Cagampan, E., Min, N., Güney, E., *et al.* (2022) Regulation of liver subcellular architecture controls metabolic homeostasis. *Nature.* **603**, 736–742